Small-angle solution scattering: from fundamental theory to practical approximations

Kristian Lytje and Jochen S. Hub

*Theoretical Physics and Center for Biophysics, Universität des Saarlandes, Saarbrücken, Germany**

Jan Skov Pedersen

Department of Chemistry and Interdisciplinary Nanoscience Center (iNANO), Aarhus University, Aarhus, Denmark

arXiv:2606.05007v1 [physics.bio-ph] 3 Jun 2026

Small-angle scattering (SAS) is widely used in structural biology, soft matter, and colloidal science to probe molecular structures in solution. SAS rests on a single physical principle: wave interference from a distribution of scatterers, averaged over orientations. Yet the theoretical foundations of SAS are spread across the literature, often based on differing notation, definitions, and implicit assumptions. We present the theory of SAS in solution from first principles as a continuous derivation, spanning the scattering of a single electron to the observed intensity of a molecular solution and its comparison with atomistic structural models. The derivation is explicit throughout—approximations, averaging procedures, and algebraic manipulations are stated rather than assumed—and is independent of the probe (X-ray or neutron) and applicable to both rigid and flexible molecules. The framework resolves several ambiguities in the current literature, notably the role of background subtraction as a theoretical rather than a purely experimental operation and the role of boundary cross-terms in justifying that subtraction. A central result is that analytical scattering calculations and approaches based on explicit-solvent molecular dynamics, typically treated as distinct traditions, are realizations of the common theoretical framework derived here. As the precision and reproducibility of SAS data continue to increase, this unified framework provides a basis for integrating theory, simulation, and experiment in future developments of SAS.

I. INTRODUCTION

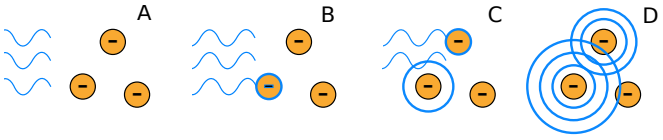
Small-angle scattering (SAS) is among the most widely used techniques for probing the structure of matter under solution conditions. By measuring the intensity of X-rays or neutrons scattered at small angles from a solution, SAS reveals ensemble-averaged structural information about systems—biomolecules, polymer assemblies, complex fluids—that resist crystallization or are too disordered for high-resolution imaging. Across the broad range of applications in structural biology, soft-condensed-matter physics, and colloidal science, SAS rests on a simple physical principle: the observed intensity arises from wave interference from a spatial distribution of scatterers, averaged over orientation. The full formal structure of the technique follows from this principle.

In practice, however, this simple foundation is difficult to grasp because the theory of SAS is distributed across a scattered literature: the scattering amplitude is derived in one source, the treatment of solvent contrast in another, background subtraction in a third (typically as an experimental prescription rather than a theoretical step), and the connection to explicit-solvent molecular-dynamics (MD) simulations in a fourth, with notation and definitions that differ between sources and assumptions that are rarely made explicit. This fragmentation has consequences. The two subtraction schemes used in practice—direct and volume-corrected—are routinely applied as if interchangeable, despite embedding different physical approximations with different validity limits. Likewise, conventional modeling approaches and those based on MD simulations are treated in the literature as distinct traditions, despite describing the same underlying physics.

The present work develops the theory of small-angle scattering from first principles as a single, continuous derivation, spanning the scattering of a single electron to the measured intensity of a multi-molecular solution and its comparison with atomistic structural models. Three commitments shape this development. First, the full range of SAS applications—analytical form factors, solution scattering, background subtraction, and atomistic modeling—is derived explicitly from the same underlying interference formalism, rather than being introduced as separate constructions. Second, the emphasis throughout is on intuition and fully worked

* kristian.lytje@uni-saarland.de, jochen.hub@uni-saarland.de

FIG. 1 Illustration of X-ray scattering: (A) an incoming plane wave, (B) scattering from an electron, (C) creating a secondary spherical wave, (D) interfering with another scattered wave.



derivations: every approximation is motivated, every averaging procedure is made explicit, and no step is relegated to a convention. Third, the formalism is developed generally, applying equally to rigid and flexible molecules, to homogeneous and heterogeneous systems, and to both X-ray and neutron scattering.

The paper is organized in two halves. The first half, comprising Sections II–IV, derives the observable SAS signal, starting from scattering by electrons and building up to atoms, molecules, and molecular ensembles, before treating the modification of these results by uniform and structured solvents. This development culminates in a formal derivation of the background-subtraction schemes used in practice, together with the approximations on which they rely. The second half turns to modeling. Section V discusses approaches that require no prior atomistic structure: model-independent analysis, the pair-distance distribution function, and analytical scattering models for idealized shapes. Section VI addresses SAS modeling for cases where an atomistic reference structure is available. This section connects these methods to MD-based scattering calculations and establishes their formal equivalence. The result is a single theoretical foundation from which the apparent diversity of SAS methods—analytical, numerical, and explicit-solvent—emerges as different routes through the same underlying physics.

SANS The theoretical framework developed here applies equally to X-ray and neutron scattering; we adopt X-ray terminology for concreteness, with neutron-specific substitutions noted where relevant.

II. SCATTERING IN VACUUM

Small-angle scattering is governed by *diffraction*: the interference of scattered waves. A useful way to visualize this is to imagine an ocean wave approaching a rocky shoreline. When the wave hits a cliff, it does not simply vanish; instead, it generates circular ripples radiating outward. As these ripples from different cliffs overlap, they interfere: where crest meets crest, the water rises higher; where crest meets trough, they cancel out. This *interference* between waves results in a complex pattern undulating on the ocean surface.

This picture is analogous to how X-rays and neutrons interact with matter. When an incident beam of radiation encounters an electron (or a nucleus), it is scattered in all directions as a secondary wave. Since this happens at many scattering centers simultaneously, the outgoing waves overlap and interfere, giving rise to the patterns measured in small-angle scattering and crystallography. See Fig. 1 for an illustration of this process.

To formalize the intuition, consider the scattering of an incident beam by an electron. Because the source is far from the sample, the incident wave appears locally planar at the scattering site. The scattered wave, in contrast, propagates outward as a spherical wave. In the far-field with large distances r, the total wave function thus takes the standard asymptotic form:

$$\psi(\boldsymbol{r}) = e^{i\boldsymbol{k}_{\text{in}}\cdot\boldsymbol{r}} + A(\theta,\phi)\frac{e^{ik_{\text{out}}r}}{r} \tag{1}$$

where $\boldsymbol{k}_{\text{in}} = k_{\text{in}}\hat{z}$ is the incident wave vector, assumed parallel to the z axis, and (θ,ϕ) are the polar and azimuthal angles of the outgoing wave vector $\boldsymbol{k}_{\text{out}}$. The first term represents the incident plane wave, while the second term describes the outgoing spherical wave, modulated by the angle-dependent *scattering amplitude* $A(\theta,\phi)$. This function encapsulates all information accessible in scattering experiments and is central to this work.

A. Fundamental quantities for small-angle scattering

1. The scattering vector

In small-angle scattering, we are primarily concerned with *elastic* scattering, where the photon changes direction but not energy. The incident photon may then be modeled as a particle interacting with an electron, after which it is deflected into a new direction determined by the scattering amplitude $A(\theta,\phi)$.

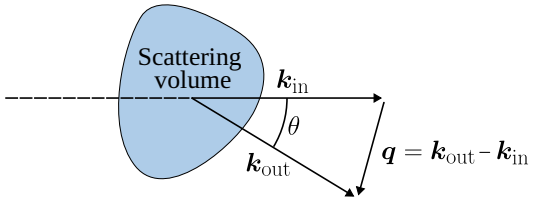
The change in momentum is described by the *momentum transfer* vector, also called the *scattering vector*, denoted by $\boldsymbol{q}$. It is defined as the difference between the outgoing and incoming wave vectors:

$$|\boldsymbol{q}|^2 = |\boldsymbol{k}_{\text{out}} - \boldsymbol{k}_{\text{in}}|^2 = |\boldsymbol{k}_{\text{out}}|^2 + |\boldsymbol{k}_{\text{in}}|^2 - 2|\boldsymbol{k}_{\text{out}}||\boldsymbol{k}_{\text{in}}|\cos\theta$$

where θ is the scattering angle between the two wave vectors (Fig. 2).

For elastic scattering, the magnitudes of the wave vectors are equal: $|\boldsymbol{k}_{\text{in}}| = |\boldsymbol{k}_{\text{out}}| = 2\pi/\lambda$, where λ is the wavelength of the radiation (electromagnetic for X-rays, de

FIG. 2 Geometry of the scattering vector $\boldsymbol{q}$. An incoming photon with wave vector $\boldsymbol{k}_{\text{in}}$ is scattered into $\boldsymbol{k}_{\text{out}}$, with $\boldsymbol{q} = \boldsymbol{k}_{\text{out}} - \boldsymbol{k}_{\text{in}}$.



Broglie for neutrons). Substituting this gives:

$$|\boldsymbol{q}| = \frac{4\pi}{\lambda}\sqrt{\frac{1-\cos\theta}{2}} = \frac{4\pi}{\lambda}\sin\frac{\theta}{2}$$

This result may also be derived from the scattering geometry shown in Fig. 2. Expressing the measured quantity in terms of $|\boldsymbol{q}|$ is convenient because it absorbs the experiment-specific values of λ and θ, allowing direct comparison across different experimental setups. Accordingly, we express scattering quantities as functions of $\boldsymbol{q}$ rather than (θ, ϕ) throughout the remainder of this work.

Inelastic scattering, where both energy and momentum are exchanged (e.g. Raman and Compton scattering), also occurs but is typically removed experimentally for X-rays (Jeffries *et al.*, 2021; Svergun *et al.*, 2013). For neutrons it can be substantial in absolute terms, but in solution measurements it originates predominantly from the buffer (Barker and Mildner, 2015) and therefore mostly cancels in the background subtraction (Sec. IV). We will therefore not consider inelastic scattering further in this work.

2. The scattering intensity

The scattering amplitude $A(\theta, \phi)$ describes the angular distribution of scattered photons and is therefore directly related to the probability of scattering in a given direction. Specifically, the differential cross-section $d\sigma/d\Omega$, which quantifies the probability of scattering into a unit solid angle for a single particle, is proportional to the squared amplitude (Sakurai and Napolitano, 2017):

$$\frac{d\sigma}{d\Omega} \propto |A(\boldsymbol{q})|^2$$

Experimentally, the detector measures the number of photons scattered into a given direction, so the observed intensity $I(\boldsymbol{q})$ is proportional to the differential cross-section and thus to the squared amplitude:

$$I(\boldsymbol{q}) = |A(\boldsymbol{q})|^2 \tag{2}$$

Here, we have dropped the proportionality constant for brevity. Although intensity is what we measure, interference occurs at the amplitude level. Therefore, for modeling SAS experiments, the general strategy is:

Compute total amplitude $A(\boldsymbol{q}) \rightarrow$ Square it to obtain $I(\boldsymbol{q})$

At this stage, $I(\boldsymbol{q})$ still depends on the azimuthal angle ϕ through $\boldsymbol{q}$. Later, we will remove this dependence by orientational averaging, after which the intensity is written as $I(q)$.

B. Scattering by an atom

We now turn to the description of molecular scattering, beginning with the case of scattering in vacuum. This serves as the foundation for the more complex scenario of macromolecules in solution addressed further below.

A first-principles derivation of scattering theory would begin with the Schrödinger equation. However, to keep this review accessible, we will omit the quantum-mechanical derivations and instead start from the Born series. Readers interested in the intermediate steps are referred to standard quantum mechanics texts such as Sakurai and Napolitano (2017) or Griffiths and Schroeter (2018).

For systems containing multiple electrons, a single photon could, in principle, scatter more than once, which would greatly complicate the analysis. However, as the scattering cross section is relatively small under typical experimental conditions even for neutrons (Barker and Mildner, 2015), such consecutive scattering events are rare and may be neglected. Assuming additionally that the incident wave propagates through the sample essentially unperturbed—the *first Born approximation*—and neglecting polarization and magnetic effects, the far-field scattering amplitude reduces to the Fourier transform of the local interaction potential (Born, 1926):

$$A(\boldsymbol{q}) = \int_V \rho(\boldsymbol{r}) e^{i\boldsymbol{q}\cdot\boldsymbol{r}} d\boldsymbol{r} \tag{3}$$

where the integral runs over the entire scattering volume, and $\rho(\boldsymbol{r})$ is the local interaction potential.

When evaluated for a single atom, this amplitude is commonly referred to as the *atomic form factor*, $f(\boldsymbol{q})$. These form factors have been extensively studied and tabulated in resources such as the International Tables for Crystallography (Prince, 2004) and Sears (1992).

SAXS For X-rays, the interaction potential depends almost entirely on the electron distribution, as the contribution from protons is negligible due to their larger mass (de Jeu (2016)). The scattering density is there-

fore well described by the electron density:

$$\rho(\boldsymbol{r}) \propto \rho_e(\boldsymbol{r})$$

Evaluating Eq. 3 at $q = 0$ then gives the total number of electrons, equal to the atomic number Z.[a]

Assuming the electron density of the atom is spherically symmetric, the scattering becomes independent of the azimuthal angle ϕ around the beam direction. Consequently, X-ray form factors are typically tabulated as a function of the magnitude $q \equiv |\boldsymbol{q}|$.

Deviations from spherical symmetry can occur near atomic bonds, where neighboring nuclei perturb the electron distribution. These deviations provide valuable insight into bonding and electronic structure. Techniques such as *anisotropic scattering* and *resonant X-ray scattering* exploit these effects to probe chemical bonding.

SANS For neutrons, the interaction potential is expressed as the scattering length density:

$$\rho(\boldsymbol{r}) \propto b(\boldsymbol{r})$$

which varies with atomic species and isotope.

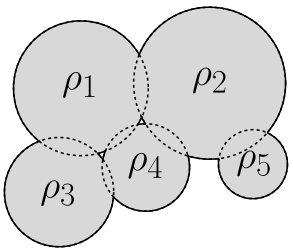
Because nuclei appear effectively point-like relative to the neutron wavelength, they present no internal structure to the probe, and atomic scattering is therefore isotropic. Neutron form factors are nearly constant throughout the small-angle q-range and are thus usually tabulated as fixed values for each isotope.

Magnetic scattering can be treated similarly by introducing a magnetic interaction potential in the Born approximation (Mühlbauer *et al.*, 2019; Wiedenmann, 2001), though this possibility will not be discussed further here.

C. Scattering by a molecule

We now extend our discussion from individual atoms to larger assemblies, such as composite particles or biomolecules. The collective scattering amplitude, still denoted $A(\boldsymbol{q})$, is often called the *molecular form factor*, while the contribution from a single atom is denoted as the atomic form factor introduced above.

FIG. 3 A system of five overlapping spherical scatterers, each with density ρ_i centered at $\boldsymbol{r}_i$. The total density is given by Eq. 4.



$$\rho_{\mathrm{m}}(\boldsymbol{r}) = \rho_1(\boldsymbol{r} - \boldsymbol{r}_1) + \rho_2(\boldsymbol{r} - \boldsymbol{r}_2) + \ldots$$

The general expression for the scattering amplitude (Eq. 3) remains valid for any scattering object; the distinction lies solely in the integration volume of the density function. Although this generality holds for many of our later derivations, we will consistently refer to the scattering objects as "atoms" and "molecules" for clarity.

1. Summing over individual atoms

For a system composed of multiple atoms, each with density $\rho_i(\boldsymbol{r})$, the total electron density is the sum over individual atomic densities, each centered on its position $\boldsymbol{r}_i$:

$$\rho_{\mathrm{m}}(\boldsymbol{r}) = \sum_i \rho_i(\boldsymbol{r} - \boldsymbol{r}_i) \tag{4}$$

with the subscript "m" denoting the density of a single molecule. This situation is illustrated in Fig. 3, where five overlapping spherical scatterers contribute to the total density.

Inserting this into Eq. 3 yields:

$$A_{\mathrm{m}}(\boldsymbol{q}) = \int_V \sum_i \rho_i(\boldsymbol{r} - \boldsymbol{r}_i) e^{i\boldsymbol{q}\cdot\boldsymbol{r}} d\boldsymbol{r}$$

Because the Fourier transform is linear, the sum can be taken outside the integral:

$$\begin{aligned} A_{\mathrm{m}}(\boldsymbol{q}) &= \sum_i \int_V \rho_i(\boldsymbol{r} - \boldsymbol{r}_i) e^{i\boldsymbol{q}\cdot\boldsymbol{r}} d\boldsymbol{r} \\ &= \sum_i e^{i\boldsymbol{q}\cdot\boldsymbol{r}_i} \int_V \rho_i(\boldsymbol{r}_i') e^{i\boldsymbol{q}\cdot\boldsymbol{r}_i'} d\boldsymbol{r}_i' \\ &= \sum_i e^{i\boldsymbol{q}\cdot\boldsymbol{r}_i} f_i(\boldsymbol{q}) \end{aligned} \tag{5}$$

where we used the substitution $\boldsymbol{r}_i' = \boldsymbol{r} - \boldsymbol{r}_i$. This fundamental result shows that the total scattering amplitude

[1] Some references absorb the classical electron (Thomson) radius r_e into the proportionality, $\rho(\boldsymbol{r}) = r_e \rho_e(\boldsymbol{r})$, to align the units of the scattering amplitude with Eq. 1 and the customary scattering length density convention used in the neutron scattering literature.

is a sum of contributions from all atoms, each described by two components:

- The **atomic form factor** $f_i(\boldsymbol{q})$ captures the intrinsic scattering of the individual atom due to its shape, size, and internal structure, as determined by its local density distribution.
- The **phase term** $e^{i\boldsymbol{q}\cdot\boldsymbol{r}_i}$ accounts for how these contributions interfere due to the spatial arrangement of the atoms (cf. the ocean-and-cliffs analogy: the resulting wave pattern depends not only on the shape of each cliff but also on their relative positions along the shoreline).

This decomposition is powerful because it separates internal atomic structure from the overall molecular geometry. The former is captured by the form factor, while the latter is described by the phase term. The same expression applies to any collection of scatterers, not only atoms. As noted above, Eq. 3 places no restriction on the integration volume, so $f_i(\boldsymbol{q})$ and $\boldsymbol{r}_i$ in Eq. 5 may equally be taken as the form factor and position of a molecule, a domain, or any other scattering object, yielding the scattering amplitude of an ensemble of such objects.

D. Scattering by multiple molecules

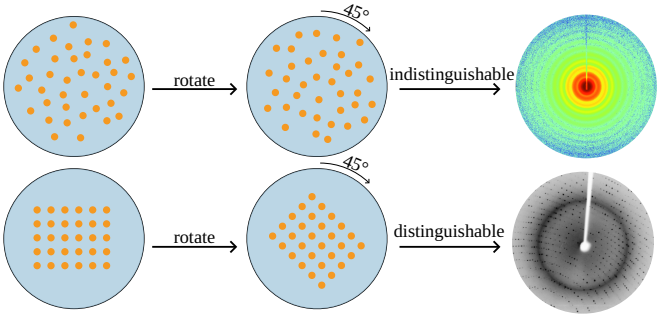
When the beam interacts with a sample containing many molecules, the measured intensity reflects the combined scattering from all molecules in the illuminated volume. In principle, the observed scattering depends on both the position and orientation of every molecule; a prohibitively complex problem for most systems. To make progress, we adopt a statistical approach: rather than modeling each molecule individually, we approximate the ensemble by a single representative structure. Quantities computed from this structure are indicated by an asterisk (*).

This approximation works well for rigid globular systems and remains reasonable for moderately flexible or disordered systems. When it fails, such as in solutions containing dynamic oligomers, multiple average structures can be used, weighted by their relative populations. For highly flexible systems, the ensemble average can be computed over many conformations, typically obtained from statistical models, molecular dynamics simulations, or ensemble refinement; see Sec. VI.B.4.

1. Symmetries and angular dependence

Let us consider a collection of molecules arranged in space. When the beam interacts with this assembly, the scattered intensity depends on the relative positions and orientations of the molecules. At this stage, there is no inherent reason to assume that the resulting interference pattern will exhibit any particular symmetry.

FIG. 4 The role of rotational invariance in scattering. The top panel shows radially symmetric SAXS rings; the bottom panel shows discrete Bragg spots from a crystal. SAXS and crystallography data adapted from Narayanan *et al.* (2018) and Sader *et al.* (2009).



To make this dependence more concrete, imagine keeping the sample fixed while rotating the detector around the beam axis. If the molecular arrangement lacks rotational symmetry, this rotation changes the relative orientation between the beam and the molecular geometry, altering the interference pattern. In the general case, the scattering intensity therefore depends on both the polar angle θ and the azimuthal angle ϕ.

Two limiting cases illustrate this principle:

- *Crystals*: Their ordered lattice introduces preferred directions, breaking rotational symmetry about the beam axis. Rotating the detector (or equivalently, the sample) changes the interference conditions, and thus Bragg spots depend on both θ and ϕ.
- *Dilute solutions*: Randomly oriented and isotropically distributed molecules are invariant under rotation about the beam axis; the rotated system is indistinguishable from the original. This rotational symmetry forces the observed intensity to be independent of the azimuthal angle, leaving only a radial dependence on the scattering vector. The resulting interference pattern is radially symmetric, forming continuous rings rather than discrete spots (Fig. 4). When isotropy is violated— e.g. due to intermolecular interactions or flow-induced alignment, particularly for anisotropic molecules—dependence on the azimuthal angle reappears.

2. Scattering by *uncorrelated* molecules

Many SAS experiments are performed on dilute solutions, where intermolecular interactions are negligible.

We refer to such cases as *uncorrelated* systems.

Using Eq. 5 to compute the scattering amplitude of multiple molecules rather than multiple atoms, the amplitude of the system becomes $A_\mathrm{s}(\boldsymbol{q}) = \sum_i A_\mathrm{m}(\boldsymbol{q}, \omega_i) e^{i\boldsymbol{q}\cdot\boldsymbol{r}_i}$, where ω_i denotes the conformation and orientation of molecule i and the subscript "s" denotes the entire system. Squaring to obtain the intensity:

$$I_\mathrm{s}(q) = |A_\mathrm{s}(\boldsymbol{q})|^2 = \sum_{ij}^{N} A_\mathrm{m}(\boldsymbol{q}, \omega_i) \bar{A}_\mathrm{m}(\boldsymbol{q}, \omega_j) e^{i\boldsymbol{q}\cdot\boldsymbol{r}_{ij}}$$

where $\bar{A}$ is the complex conjugate. Splitting the sum into self-terms ($i = j$) and cross-terms ($i \neq j$):

$$\begin{aligned} I_\mathrm{s}(q) &= \sum_{i}^{N} |A_\mathrm{m}(\boldsymbol{q}, \omega_i)|^2 + \sum_{i\neq j}^{N} A_\mathrm{m}(\boldsymbol{q}, \omega_i) \bar{A}_\mathrm{m}(\boldsymbol{q}, \omega_j) e^{i\boldsymbol{q}\cdot\boldsymbol{r}_{ij}} \\ &= \sum_{i}^{N} |A^*_\mathrm{m}(\boldsymbol{q}, \omega_i)|^2 + \sum_{i\neq j}^{N} A^*_\mathrm{m}(\boldsymbol{q}, \omega_i) \bar{A}^*_\mathrm{m}(\boldsymbol{q}, \omega_j) e^{i\boldsymbol{q}\cdot\boldsymbol{r}_{ij}} \end{aligned}$$

where in the second equality we have replaced each molecule by the representative structure, so that ω_i now describes orientation alone rather than both conformation and orientation. Under this approximation, the sum over self-terms is self-averaging: it uniformly samples all orientations of the same molecular structure N times. Thus:

$$I_\mathrm{s}(q) = N\langle |A^*_\mathrm{m}(\boldsymbol{q}, \omega_i)|^2 \rangle_\Omega + \sum_{i\neq j}^{N} A^*_\mathrm{m}(\boldsymbol{q}, \omega_i) \bar{A}^*_\mathrm{m}(\boldsymbol{q}, \omega_j) e^{i\boldsymbol{q}\cdot\boldsymbol{r}_{ij}}, \tag{6}$$

where $\langle\cdot\rangle_\Omega$ denotes the orientational average. In a dilute solution, the orientations ω_i and ω_j of different molecules are independent and uniformly distributed, and are independent of the separation vector r_{ij}. The cross-term is therefore also self-averaging: for each fixed orientation ω_i, all orientations ω_j and distances r_{ij} are sampled with equal probability. The cross-term may therefore be simplified to the following:

$$\begin{aligned} I_\mathrm{s}(q) &= N\langle |A^*_\mathrm{m}(\boldsymbol{q})|^2 \rangle_\Omega \\ &\quad + N(N-1)\langle A^*_\mathrm{m}(\boldsymbol{q})\rangle_\Omega \langle \bar{A}^*_\mathrm{m}(\boldsymbol{q})\rangle_\Omega \langle e^{i\boldsymbol{q}\cdot\boldsymbol{r}}\rangle_\Omega \\ &= N\langle |A^*_\mathrm{m}(\boldsymbol{q})|^2 \rangle_\Omega + |\langle A^*_\mathrm{m}(\boldsymbol{q})\rangle_\Omega|^2 \sum_{i\neq j}^{N} \langle e^{i\boldsymbol{q}\cdot\boldsymbol{r}_{ij}}\rangle_\Omega \end{aligned}$$

With no preferred orientation or separation, the phase factors fluctuate randomly, and their orientational average cancels out:[2]

$$I_\mathrm{s}(q) = N\langle |A^*_\mathrm{m}(\boldsymbol{q})|^2 \rangle_\Omega \equiv N I^*_\mathrm{m}(q) \quad \text{(uncorrelated)} \tag{7}$$

This result is useful as it shows that, for dilute solutions of nearly identical, non-interacting molecules, the total intensity equals the number of molecules multiplied by the intensity from a single molecule.

In the literature, this result is often written as $I_\mathrm{s}(q) = NP(q)$, where $P(q)$ is also referred to as the molecular form factor. Since $P(q)$ is an orientationally averaged intensity rather than a scattering amplitude, we will avoid this terminology here.

3. Scattering by *correlated* molecules

When the spatial positions of the molecules are correlated, for example due to intermolecular interactions, the second term in Eq. 6 must be retained. However, this term cannot be evaluated without detailed knowledge of the interaction potential. To address this, various approximation schemes have been proposed (Pedersen, J.S. in Lindner and Oberdisse (2024)); here, we use the simplest of these: the *decoupling approximation* proposed by Kotlarchyk and Chen (1983). This approximation assumes that molecular orientations are independent of positions and of each other; interactions affect where molecules sit, not how they point.

Applying this approximation, the orientational and positional averages decouple, returning us to the form of Eq. 6:

$$\begin{aligned} I_\mathrm{s}(q) &= N\langle |A^*_\mathrm{m}(\boldsymbol{q})|^2 \rangle_\Omega + |\langle A^*_\mathrm{m}(\boldsymbol{q})\rangle_\Omega|^2 \sum_{i\neq j}^{N} \left\langle e^{i\boldsymbol{q}\cdot\boldsymbol{r}_{ij}} \right\rangle_\Omega \\ &= N\langle |A^*_\mathrm{m}(\boldsymbol{q})|^2 \rangle_\Omega \left\{ 1 + \frac{|\langle A^*_\mathrm{m}(\boldsymbol{q})\rangle_\Omega|^2}{\langle |A^*_\mathrm{m}(\boldsymbol{q})|^2 \rangle_\Omega} \frac{1}{N} \sum_{i\neq j}^{N} \left\langle e^{i\boldsymbol{q}\cdot\boldsymbol{r}_{ij}} \right\rangle_\Omega \right\} \end{aligned}$$

This motivates the definition of the *structure factor*:

$$S^*(q) \equiv 1 + \frac{\beta^*(q)}{N} \sum_{i\neq j}^{N} \left\langle e^{i\boldsymbol{q}\cdot\boldsymbol{r}_{ij}} \right\rangle_\Omega \qquad \beta^*(q) = \frac{|\langle A^*_\mathrm{m}(\boldsymbol{q})\rangle_\Omega|^2}{\langle |A^*_\mathrm{m}(\boldsymbol{q})|^2 \rangle_\Omega}$$

where we have introduced $\beta^*(q)$ for convenience. The intensity then takes the form:

$$I_\mathrm{s}(q) = N\langle |A^*_\mathrm{m}(\boldsymbol{q})|^2 \rangle_\Omega S^*(q) = N I^*_\mathrm{m}(q) S^*(q) \quad \text{(correlated)} \tag{8}$$

---

[2] Strictly speaking, the phase-cancellation argument does not apply in the limit $q \to 0$, where $e^{i\boldsymbol{q}\cdot\boldsymbol{r}_{ij}} \to 1$ for all pairs. In this limit, scattering probes particle-number fluctuations within the illuminated volume rather than local spatial correlations, and the structure factor is fixed by the isothermal compressibility via $S(0) = nk_\mathrm{B}T\kappa_T$.

Under this approximation, the observed intensity is that of the dilute case but modulated by the structure factor, which captures the effect of molecular correlations. The structure factor is commonly evaluated using correlation functions, which we explore in App. A1.

4. When to account for the structure factor

The structure factor must be considered whenever interparticle interactions produce non-random spatial correlations, such as in concentrated solutions, aggregated systems, or in samples exhibiting strong long-range repulsion. In these cases, $S^*(q)$ must be modeled or computed using additional information about the system (L. Cipelletti, R. Klein, and E. Zaccarelli in Lindner and Oberdisse (2024)). For dilute solutions, these interactions are negligible, and $S^*(q) \approx 1$ can be assumed, reducing the analysis to the uncorrelated case described earlier.

Since the structure factor always appears as a multiplicative term with the intensity $I^*_{\mathrm{m}}(q)$, we will omit it for brevity.

5. Evaluating $I^*_{\mathrm{m}}(q)$: the Debye equation

In both the correlated and uncorrelated cases described above, the total scattering depends on the orientationally averaged single-molecule intensity $I^*_{\mathrm{m}}(q)$. When an atomistic structure is available, it can be computed analytically by averaging the phase factors in Eq. 5 over all molecular orientations to obtain a central equation in SAS: the Debye equation.

To derive it, we start by computing the orientational average of the exponential term in Eq. 5. Since the integrand depends only on the relative angle between $\boldsymbol{q}$ and $\boldsymbol{r}$, the average can be carried out either with $\boldsymbol{q}$ fixed and $\boldsymbol{r}$ averaged over orientations, denoted $\langle\cdot\rangle_{\Omega_r}$, or vice versa, denoted $\langle\cdot\rangle_{\Omega_q}$; see Sec. V.C.3. The two are equivalent, and we write $\langle\cdot\rangle_\Omega$ throughout when the distinction is immaterial. Aligning the polar axis with the fixed vector gives $\boldsymbol{q}\cdot\boldsymbol{r} = qr\cos\vartheta$, and the average reduces to an integral in polar coordinates (ϑ, φ):

$$\begin{aligned}\left\langle e^{i\boldsymbol{q}\cdot\boldsymbol{r}}\right\rangle_\Omega &= \frac{1}{4\pi}\int_0^{2\pi} d\varphi \int_0^{\pi} \sin\vartheta\, e^{iqr\cos\vartheta} d\vartheta \\ &= \frac{1}{2}\int_{-1}^{1} e^{iqrx} dx = \frac{\sin qr}{qr} \equiv \operatorname{sinc} qr \end{aligned} \tag{9}$$

where we have used the substitution $x = \cos\vartheta$. This term represents the orientationally averaged phase factor between two scatterers separated by distance r. It equals the zeroth-order spherical Bessel function $j_0(qr)$, a notation often used in the modeling literature. A commonly used alternative to this analytical average is to expand the phase into a spherical harmonics basis, as described in App. A2.

TABLE I Notation used in this paper. Subscript "s" denotes the entire system (molecules + buffer), "b" the buffer region, "m" a single molecule, and "M" all molecules; they are capitalized in volumes for clarity in nested subscripts. See Fig. 6 for a visual overview.

Subscript	s	b	M	m
Meaning	System	Buffer	All molecules	Single molecule
Volume	V_{S}	V_{B}	$V_{\mathrm{M}} = V_{\mathrm{S}} - V_{\mathrm{B}}$	$V_{\mathrm{m}} = V_{\mathrm{M}}/N$

Next, from the squared and orientationally averaged amplitude of Eq. 5:

$$I^*_{\mathrm{m}}(q) = \langle |A^*_{\mathrm{m}}(\boldsymbol{q})|^2\rangle_\Omega = \sum_{ij}^{N} \left\langle f_i(\boldsymbol{q}) f_j(\boldsymbol{q}) e^{i\boldsymbol{q}\cdot\boldsymbol{r}_{ij}}\right\rangle_\Omega$$

For structures composed of individual atoms, the form factors depend only on the magnitude of $\boldsymbol{q}$, so $f(\boldsymbol{q}) = f(q)$.[3] Using this assumption, the average can be evaluated analytically to yield the Debye equation (Debye, 1915):

$$\begin{aligned} I^*_{\mathrm{m}}(q) &= \sum_{ij}^{N} f_i(q) f_j(q) \left\langle e^{i\boldsymbol{q}\cdot\boldsymbol{r}_{ij}}\right\rangle_\Omega \\ &= \sum_{ij}^{N} f_i(q) f_j(q) \operatorname{sinc} qr_{ij} \end{aligned} \tag{10}$$

where $r_{ij} \equiv |\boldsymbol{r}_{ij}|$ is the distance between atoms i and j. This equation provides an exact expression for the orientationally averaged scattering resulting from any atomistic structure, regardless of its symmetry or internal complexity.

III. SCATTERING BY SOLUTIONS

Up to this point, we assumed that the molecules are suspended in vacuum. However, in nearly all SAS experiments (see Fig. 5), there is a solvent present which dominates the observed scattering signal. Understanding and accounting for the solvent contribution is the focus of this section.

To formalize the discussion, we adopt the notation summarized in Table I. The term *buffer* denotes the surrounding solution in which the molecules are embedded,

[3] While we here derive it for atoms, the Debye equation also holds for larger constituents provided they are spherically symmetric and $f(\boldsymbol{q}) = f(q)$.

FIG. 5 A simplified view of a typical experimental setup. A monochromatic X-ray beam is collimated by apertures before scattering off the electrons in the sample at an angle 2θ, producing an azimuthally symmetric diffraction pattern. Figure adapted with permission from Als-Nielsen and McMorrow (2011).

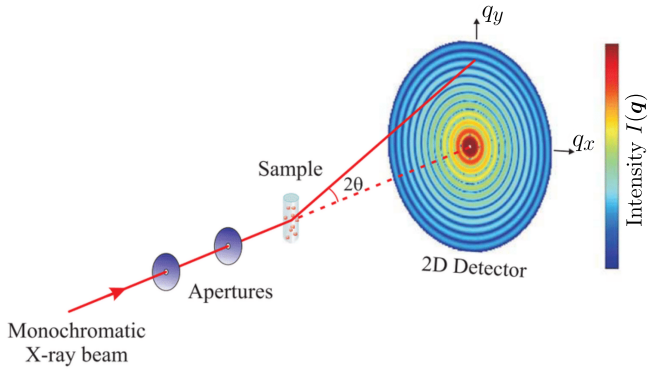
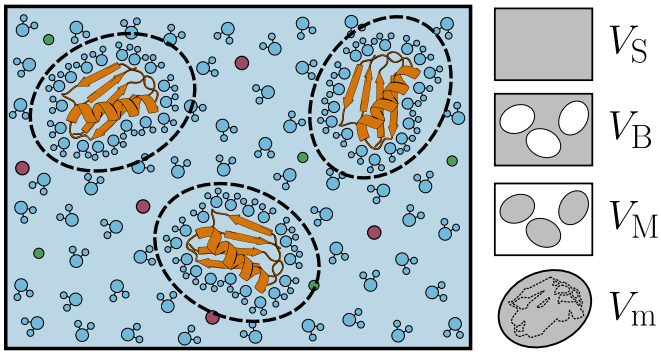


FIG. 6 Visual overview of the notation used in this paper. The system volume is denoted by V_S, volume of all molecules by V_M, and volume per molecule by V_m. The buffer region is denoted as either V_B or the complement $V_\mathrm{M}^\complement$ of V_M depending on context. The exact boundary of V_m will be clarified later.



while *system* refers to the complete ensemble comprising both molecules and buffer.

We begin with the simplest case: a solvent of uniform density, that is, without any internal structure. Examining this idealized system will help to understand the baseline effect of solvent on the observed scattering. In Sec. III.C, we will extend the analysis to inhomogeneous solvents, accounting for both local density variations and time-dependent fluctuations.

A. Scattering by uniform solvents

A fundamental principle of small-angle scattering is that only spatial variations in electron density contribute to the measured signal. To see why, consider a system of perfectly uniform density. The scattered waves from every point would have identical amplitudes but different phases, leading to complete destructive interference, except at $\boldsymbol{q} = 0$ (Fig. 7A). Only scattering from the boundary region near the container walls would be observed. However, when a local density variation is introduced (Fig. 7B and C), the uniformity is broken, and the scattered waves no longer cancel. Such variations are the source of the SAS signal.

This intuition can be formalized by computing the scattering amplitude of a uniform density ρ_b. Substituting $\rho(\boldsymbol{r}) = \rho_\mathrm{b}$ into Eq. 3 and integrating over the system volume gives:

$$A_\mathrm{s}(\boldsymbol{q}) = \rho_\mathrm{b} \int_{V_\mathrm{S}} e^{i\boldsymbol{q}\cdot\boldsymbol{r}} d\boldsymbol{r} = \rho_\mathrm{b} \mathcal{S}_{V_\mathrm{S}}(\boldsymbol{q}) \tag{11}$$

where $\mathcal{S}_{V_\mathrm{S}}(\boldsymbol{q})$ is the shape integral, describing the contribution due to the overall geometry of the scattering volume. For an infinitely large domain, this term is proportional to the Dirac delta function:

$$A_\mathrm{s}(\boldsymbol{q}) \sim \rho_\mathrm{b} \delta(\boldsymbol{q}) \tag{12}$$

Although this is only valid for an infinite domain, real systems are practically large enough that $\mathcal{S}_{V_\mathrm{S}}(\boldsymbol{q})$ contributes only within a narrow region near $\boldsymbol{q} = 0$, which is hidden behind the beamstop; a necessary component to protect the detector from direct beam exposure. Uniform densities are therefore effectively invisible in SAS experiments.

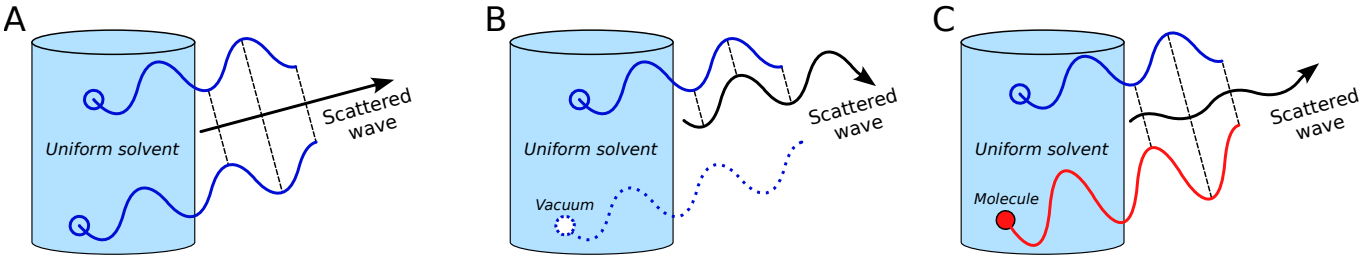
1. Scattering by a vacuum bubble: Babinet's principle

Because constant offsets in density change only forward scattering at $\boldsymbol{q} = 0$, we may freely add or subtract uniform densities without altering the observable scattering. This leads to an intuitive explanation for why a vacuum bubble scatters (Fig. 7B). Consider a system of uniform density ρ_b except for a vacuum bubble with zero density. By subtracting the uniform ρ_b, the density becomes zero in the solvent region and $-\rho_\mathrm{b}$ in the vacuum bubble. From this density-shifted perspective, only the bubble contributes to the scattering.

To formally derive this intuition, let V_V be the volume of a vacuum bubble and $V_\mathrm{V}^\complement$ its complement (the rest of the system). If the bubble were instead filled with solvent, the resulting amplitude would vanish at all relevant $\boldsymbol{q}$:

$$\rho_\mathrm{b} \int_{V_\mathrm{V}} e^{i\boldsymbol{q}\cdot\boldsymbol{r}} d\boldsymbol{r} + \rho_\mathrm{b} \int_{V_\mathrm{V}^\complement} e^{i\boldsymbol{q}\cdot\boldsymbol{r}} d\boldsymbol{r} = \rho_\mathrm{b} \int_{V_\mathrm{S}} e^{i\boldsymbol{q}\cdot\boldsymbol{r}} d\boldsymbol{r}$$
$$= \cancelto{0}{\rho_\mathrm{b} \mathcal{S}_{V_\mathrm{S}}(\boldsymbol{q})}$$

FIG. 7 Solution scattering arises from density fluctuations. (A) A perfectly uniform solution produces no net scattering. (B,C) Local density variations (e.g. molecules or voids) break uniformity, generating observable scattering.



since $\mathcal{S}_{V_S}(\boldsymbol{q})$ can be neglected, as previously argued. Rearranging, we obtain the relation:

$$\rho_b \int_{V_V^C} e^{i\boldsymbol{q}\cdot\boldsymbol{r}} d\boldsymbol{r} = -\rho_b \int_{V_V} e^{i\boldsymbol{q}\cdot\boldsymbol{r}} d\boldsymbol{r} \tag{13}$$

This confirms our intuition when applied to the vacuum-bubble system: the scattering from the uniform solvent region is equivalent to that of the bubble alone with effective density $-\rho_b$. This equivalence, first articulated by Jacques Babinet in the 19th century, is known as *Babinet's principle*, which underpins the common practice of expressing scattering in terms of excess density relative to the solvent.

2. Deriving the excess density

Next, we introduce molecules to the uniform solvent. When we earlier considered the bare molecules in vacuum, a discrete density description based on individual contributions was sufficient. Now, with the solvent occupying the space between molecules, a continuous density description is more natural. In this framework, the regions occupied by molecules (volume V_M) exhibit a spatially varying density $\rho_M(\boldsymbol{r})$, while the surrounding buffer is treated as a uniform background with density ρ_b. The system density is thus given as:

$$\rho_s(\boldsymbol{r}) = \begin{cases} \rho_M(\boldsymbol{r}) & \text{if } \boldsymbol{r} \in V_M \\ \rho_b & \text{if } \boldsymbol{r} \in V_M^C \end{cases} \tag{14}$$

The volume V_M is excluded from the buffer, as this region is already occupied by molecules. The associated scattering amplitude becomes:

$$\begin{aligned} A_s(\boldsymbol{q}) &= \int_{V_S} \rho_s(\boldsymbol{r}) e^{i\boldsymbol{q}\cdot\boldsymbol{r}} d\boldsymbol{r} \\ &= \int_{V_M} \rho_M(\boldsymbol{r}) e^{i\boldsymbol{q}\cdot\boldsymbol{r}} d\boldsymbol{r} + \rho_b \int_{V_M^C} e^{i\boldsymbol{q}\cdot\boldsymbol{r}} d\boldsymbol{r} \\ &= \int_{V_M} (\rho_M(\boldsymbol{r}) - \rho_b)\, e^{i\boldsymbol{q}\cdot\boldsymbol{r}} d\boldsymbol{r} \end{aligned}$$

where we have used Babinet's principle (Eq. 13) in the last equality. Defining the *excess density* as $\Delta\rho_M(\boldsymbol{r}) \equiv \rho_M(\boldsymbol{r}) - \rho_b$, the amplitude simplifies to:

$$A_s(\boldsymbol{q}) = \int_{V_M} \Delta\rho_M(\boldsymbol{r}) e^{i\boldsymbol{q}\cdot\boldsymbol{r}} d\boldsymbol{r} \tag{15}$$

Using Eq. 8, the intensity becomes:

$$I_s(q) = \langle |A_s(\boldsymbol{q})|^2 \rangle_\Omega = N \langle |\Delta A_m^*(\boldsymbol{q})|^2 \rangle_\Omega$$

where $\Delta A_m^*(\boldsymbol{q})$ is the amplitude corresponding to the excess density of the representative molecule, $\Delta\rho_m^*(\boldsymbol{r}) \equiv \rho_m^*(\boldsymbol{r}) - \rho_b$. Here, the asterisk $*$ again indicates the amplitude or density owing to a representative structure. Thus, for molecules in uniform solvent, the scattering depends only on the excess density $\Delta\rho_m^*(\boldsymbol{r})$ within the molecular volume. Note that the subtraction $\rho_m^*(\boldsymbol{r}) - \rho_b$ is a mathematical step, not a physical one: no second measurement is involved, and $A_s(\boldsymbol{q})$ still represents the total scattering from molecules and buffer combined.

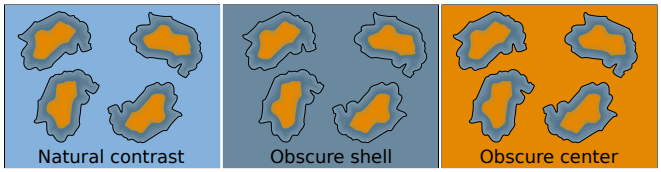
Because of the simplicity of Eq. 15, excess density alone may seem to fully describe the observed scattering. This interpretation, however, holds only for a *uniform* solvent: in real-world systems with non-uniform solvents, additional buffer contributions appear (Sec. III.C).

3. Contrast variation experiments

The excess density is historically called contrast,[4] and represents the portion of the molecular density that actually contributes to the observed scattering. As made explicit in Eq. 15, only deviations from the buffer density produce observable scattering, because any part of the

[4] The literature generally uses *contrast* with two related meanings: (i) as the average excess system density, determining the overall strength of the signal, and (ii) as a context-dependent descriptor of the relative visibility of specific molecular components under given solvent conditions.

FIG. 8 Illustration of contrast variation. By adjusting the solvent density, scattering from different molecular regions can be selectively enhanced or suppressed.



molecule matching the buffer blends into the background.

The concept of contrast underlies *contrast variation* experiments, where the buffer density is tuned such that selected molecular regions are obscured (i.e. contrast-matched and thus invisible to scattering); see Fig. 8. This approach enables targeted structural analysis of complex systems, as illustrated in the following practical implementations.

SANS Contrast variation is widely used with neutron scattering, where the different scattering lengths of hydrogen and deuterium allow control over contrast via isotopic substitution.[a] The contrast can be tuned using two complementary approaches: adjusting the H_2O/D_2O ratio in the buffer to vary its density, or by varying deuteration of specific molecular components to enhance or suppress their relative contrasts. Targeted structural analyses of individual molecular subunits are routinely performed in this manner; see Krueger (2022) for a recent review.

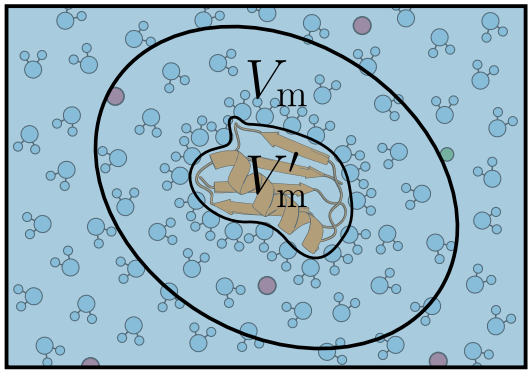
SAXS Contrast variation is more challenging with X-rays because the scattering depends on the electron density, which is harder to tune without altering molecular interactions. Traditionally, this has limited contrast variation to adding salts or sugars, though recent work employing medical contrast agents suggests potential for broader applications (Gabel *et al.*, 2022).

B. What we mean by "molecular"

Before continuing, we clarify our use of the term *molecular*. Throughout this work, the term *molecular* refers to an extended region V_m enclosing the physical molecule and its atoms (see Fig. 9). We do not specify the precise extent of V_m at this stage; it is sufficient to note that V_m extends well beyond the immediate molecular structure,

[5] Isotopic substitution requires caution, as it may alter intermolecular interactions and introduce inconsistencies ("isotope-effects") between datasets.

FIG. 9 Illustration of the difference in nomenclature. Other literature uses the label "molecular" to denote only components from the physical molecular volume V'_m. We instead use it to refer to an expanded volume V_m, whose boundary is not associated with a physical interface.



so that any structured solvent around the molecule (hydration shell) contributes to the molecular scattering I_m. This choice differs from the common convention which identifies the molecular volume with V'_m and therefore requires an explicit, molecule-dependent treatment of the hydration shell and its coupling to the bulk.

Our choice instead leads to a general framework that is agnostic not only to the internal structure and chemical composition of the molecule, but also to its shape, surface, and interaction with the solvent: all such detail is opaque to the framework and is deferred to the modeling of I_m in Sec. VI.

This distinction was irrelevant for the uniform solvents of Sec. III.A, but becomes consequential as we extend our attention to inhomogeneous solvent in the following.

C. Scattering by non-uniform solvents

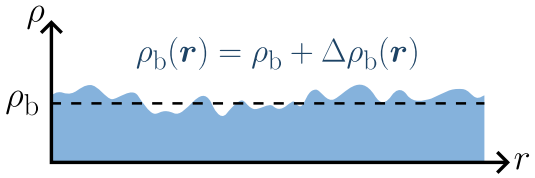
Reality is more complicated than our earlier idealization. The buffer is not a uniform medium; it consists of discrete molecules and, optionally, additives such as salt, making the buffer density inhomogeneous and subject to time-dependent density fluctuations. To account for these effects, we express the buffer density as:

$$\rho_\mathrm{b}(\boldsymbol{r},t) = \rho_\mathrm{b} + \Delta\rho_\mathrm{b}(\boldsymbol{r},t)$$

where ρ_b is the mean buffer density, and $\Delta\rho_\mathrm{b}(\boldsymbol{r},t)$ is the excess buffer density, capturing spatial and temporal fluctuations, including those from additives; see Fig. 10. The system density is then:

$$\rho_\mathrm{s}(\boldsymbol{r},t) = \begin{cases} \rho_\mathrm{M}(\boldsymbol{r},t) & \text{if } \boldsymbol{r} \in V_\mathrm{M}(t) \\ \rho_\mathrm{b}(\boldsymbol{r},t) & \text{if } \boldsymbol{r} \in V_\mathrm{B}(t) \end{cases} \tag{16}$$

FIG. 10 Decomposition of the buffer density into mean and fluctuating contributions.



Both densities and their associated volumes are considered time-dependent to account for possible molecular motion.

1. Evaluating the system intensity

We start by evaluating the intensity corresponding to the given densities. The amplitude is given by:

$$\begin{aligned} A_\mathrm{s}(\boldsymbol{q},t) &= \int_{V_\mathrm{S}} \rho_\mathrm{s}(\boldsymbol{r},t) e^{i\boldsymbol{q}\cdot\boldsymbol{r}} d\boldsymbol{r} \\ &= \int_{V_\mathrm{M}(t)} \rho_\mathrm{M}(\boldsymbol{r},t) e^{i\boldsymbol{q}\cdot\boldsymbol{r}} d\boldsymbol{r} + \int_{V_\mathrm{M}^\complement(t)} \rho_\mathrm{b}(\boldsymbol{r},t) e^{i\boldsymbol{q}\cdot\boldsymbol{r}} d\boldsymbol{r} \end{aligned}$$

where $V_\mathrm{M}(t)$ and $V_\mathrm{M}^\complement(t)$ are the (time-dependent) volumes occupied by the molecules and buffer; see Fig. 6.

Separating the buffer contribution into mean and fluctuating parts yields:

$$\begin{aligned} A_\mathrm{s}(\boldsymbol{q},t) = &\int_{V_\mathrm{M}(t)} \rho_\mathrm{M}(\boldsymbol{r},t) e^{i\boldsymbol{q}\cdot\boldsymbol{r}} d\boldsymbol{r} \\ &+ \rho_\mathrm{b} \int_{V_\mathrm{M}^\complement(t)} e^{i\boldsymbol{q}\cdot\boldsymbol{r}} d\boldsymbol{r} + \int_{V_\mathrm{M}^\complement(t)} \Delta\rho_\mathrm{b}(\boldsymbol{r},t) e^{i\boldsymbol{q}\cdot\boldsymbol{r}} d\boldsymbol{r} \end{aligned}$$

Applying Babinet's principle to invert the constant term and neglecting the forward-scattering $\mathcal{S}_{V_\mathrm{S}}(\boldsymbol{q})$ contribution:

$$\begin{aligned} A_\mathrm{s}(\boldsymbol{q},t) &= \int_{V_\mathrm{M}(t)} \rho_\mathrm{M}(\boldsymbol{r},t) e^{i\boldsymbol{q}\cdot\boldsymbol{r}} d\boldsymbol{r} \\ &\quad - \rho_\mathrm{b} \int_{V_\mathrm{M}(t)} e^{i\boldsymbol{q}\cdot\boldsymbol{r}} d\boldsymbol{r} + \int_{V_\mathrm{M}^\complement(t)} \Delta\rho_\mathrm{b}(\boldsymbol{r},t) e^{i\boldsymbol{q}\cdot\boldsymbol{r}} d\boldsymbol{r} \\ &= \int_{V_\mathrm{M}(t)} (\rho_\mathrm{M}(\boldsymbol{r},t) - \rho_\mathrm{b}) e^{i\boldsymbol{q}\cdot\boldsymbol{r}} d\boldsymbol{r} \\ &\quad + \int_{V_\mathrm{B}(t)} \Delta\rho_\mathrm{b}(\boldsymbol{r},t) e^{i\boldsymbol{q}\cdot\boldsymbol{r}} d\boldsymbol{r} \\ &= \Delta A_\mathrm{M}(\boldsymbol{q},t) + \Delta A_\mathrm{b}^{(V_\mathrm{B})}(\boldsymbol{q},t) \end{aligned} \tag{17}$$

where we have used $V_\mathrm{B}(t) \equiv V_\mathrm{M}^\complement(t)$. Here, ΔA_M and $\Delta A_\mathrm{b}^{(V_\mathrm{B})}$ are the excess molecular and buffer amplitudes, respectively (see Fig. 10), with the originating volume of the latter annotated for clarity. As expected, this result again shows that only variations in density contribute to the observable scattering.

Squaring the amplitude gives the instantaneous system intensity:

$$\begin{aligned} I_\mathrm{s}(\boldsymbol{q},t) &= |A_\mathrm{s}(\boldsymbol{q},t)|^2 \\ &= |\Delta A_\mathrm{M}(\boldsymbol{q},t) + \Delta A_\mathrm{b}(\boldsymbol{q},t)|^2 \\ &= |\Delta A_\mathrm{M}(\boldsymbol{q},t)|^2 + |\Delta A_\mathrm{b}(\boldsymbol{q},t)|^2 + \Delta C_\mathrm{M,b}^{V_\mathrm{M},V_\mathrm{B}}(\boldsymbol{q},t) \\ &= \Delta I_\mathrm{M}(\boldsymbol{q},t) + \Delta I_\mathrm{b}^{(V_\mathrm{B})}(\boldsymbol{q},t) + \Delta C_\mathrm{M,b}^{V_\mathrm{M},V_\mathrm{B}}(\boldsymbol{q},t) \end{aligned} \tag{18}$$

where the cross-term, owing to density correlations between the volumes V_M and V_B, is:

$$\begin{aligned} C_\mathrm{M,b}^{V_\mathrm{M},V_\mathrm{B}}(\boldsymbol{q},t) = &A_\mathrm{M}^{(V_\mathrm{M})}(\boldsymbol{q},t)\overline{A_\mathrm{b}^{(V_\mathrm{B})}(\boldsymbol{q},t)} \\ &+ A_\mathrm{b}^{(V_\mathrm{B})}(\boldsymbol{q},t)\overline{A_\mathrm{M}^{(V_\mathrm{M})}(\boldsymbol{q},t)} \end{aligned} \tag{19}$$

Eq. 18 expresses the instantaneous system intensity as the sum of three contributions: the excess molecular scattering $\Delta I_\mathrm{M}(\boldsymbol{q},t)$, the excess buffer scattering $\Delta I_\mathrm{b}^{(V_\mathrm{B})}(\boldsymbol{q},t)$, and the mixed term $C_\mathrm{M,b}^{V_\mathrm{M},V_\mathrm{B}}(\boldsymbol{q},t)$.

Although the explicit t-dependence could be removed by averaging over time, doing so would obscure the underlying physics by suggesting that long acquisition times are required. The vector-$\boldsymbol{q}$ dependence likewise cannot be eliminated through the usual orientational average, as the experiment probes the system in a single fixed orientation. To make progress, we therefore examine the three contributions in Eq. 18 individually to see how they may be simplified.

2. Simplifying the molecular term

Previously, we assumed all molecules shared a single representative conformation, differing only in orientation. With an explicit time dependence, this idealization no longer holds: the molecules undergo continuous thermal motion, and the instantaneous ensemble therefore spans both orientations and conformations. Evaluating $\Delta I_\mathrm{M}(\boldsymbol{q},t)$ requires averaging over this ensemble, which we denote by $\langle\cdot\rangle_N$.[6]

Due to the sheer number of molecules present in solution, every conformation is present in every orientation at any given instant. The ensemble average $\langle\cdot\rangle_N$ therefore implicitly contains an orientational average, and the

[6] In practice, the conformational average may be realized either by sampling many conformations sequentially in time, or, as is typical in SAS, by illuminating a macroscopic sample volume containing all conformations simultaneously.

result depends only on the magnitude q. Furthermore, at equilibrium the ensemble is stationary: thermal motion merely reshuffles populations among the existing states without altering their statistics. The ensemble average therefore also removes the explicit time dependence:

$$\Delta I_{\mathrm{M}}(\boldsymbol{q},t) = N\langle \Delta I^{*}_{\mathrm{m}}(\boldsymbol{q},t)\rangle_N = N\Delta I^{*}_{\mathrm{m}}(q) \tag{20}$$

3. Simplifying the buffer term

For the buffer, the conformational average used for the molecular term cannot be applied directly. Unlike the molecules, the solvent does not possess a single reference configuration: short-range solvent–solvent correlations prevent treating it as a set of independent scatterers.

Nevertheless, the buffer is an isotropic fluid at thermal equilibrium: its statistical properties do not drift with time, and they are invariant under rotations. The mean buffer signal is therefore independent of the exposure time and depends only on $|\boldsymbol{q}|$. We therefore identify the observable buffer contribution with its equilibrium mean:

$$\Delta I_{\mathrm{b}}^{(V_{\mathrm{B}})}(\boldsymbol{q},t) \longrightarrow \Delta I_{\mathrm{b}}^{(V_{\mathrm{B}})}(q). \tag{21}$$

A formal justification, which also clarifies what is meant by the usual "ensemble average" argument for a correlated bulk solvent, is given in App. A3.

4. Simplifying the cross-term

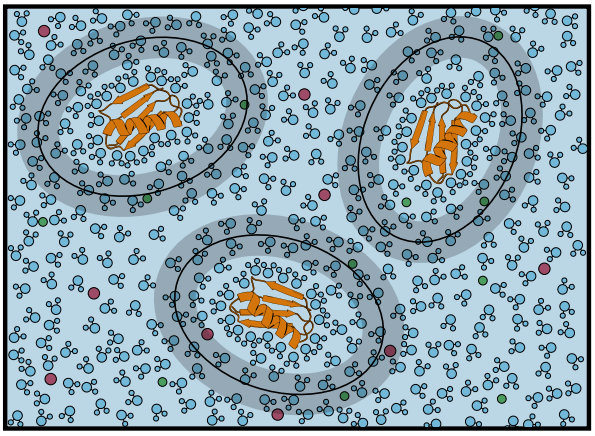
The final contribution in Eq. 18 is the cross-term $\Delta C_{\mathrm{M,b}}^{V_{\mathrm{M}},V_{\mathrm{B}}}(\boldsymbol{q},t)$, representing scattering arising from density correlations across the boundary of the molecular and buffer volumes. These correlations do not vanish: the probability of finding a solvent molecule just outside the boundary is influenced by the positions of solvent molecules just inside the boundary. The cross-term is therefore generally nonzero and cannot be neglected, as shown explicitly in App. A1.2.

The cross-term contains no self-contributions: being a product of amplitudes over disjoint volumes, all its contributions come from *correlations* between densities on the two sides of the boundary. From Sec. II.D.2, we know that uncorrelated phase factors average to zero; the cross-term therefore cannot receive contributions from regions where the densities on either side are independent. In a real solvent, density correlations are short-ranged, so only a thin shell near the boundary contributes: the interior of V_{m} plays no role.

This observation implies a practical choice for V_{m}. Provided its boundary lies in bulk solvent, i.e. far enough from the molecule that solvent–solvent correlations there are indistinguishable from those in pure buffer, the cross-term reduces to a purely bulk quantity, independent of the molecule. Under this condition, the cross-term reduces to short-range buffer–buffer contributions:

$$\Delta C_{\mathrm{M,b}}^{V_{\mathrm{M}},V_{\mathrm{B}}}(\boldsymbol{q},t) = \Delta C_{\mathrm{b,b}}^{V_{\mathrm{M}},V_{\mathrm{B}}}(\boldsymbol{q},t) \tag{22}$$

FIG. 11 Illustration of the volume partition. The system is divided into two regions separated by the solid black boundary. By making V_{m} large enough, cross-correlations across its boundary become bulk-like.



This construction is illustrated in Fig. 11, where the boundary is indicated and the correlated interfacial region contributing to $\Delta C_{\mathrm{b,b}}^{V_{\mathrm{M}},V_{\mathrm{B}}}(\boldsymbol{q},t)$ is shaded.

Because each such boundary region is associated with a single molecule, the cross-term can be simplified using the same conformational average as in Eq. 20:

$$\Delta C_{\mathrm{b,b}}^{V_{\mathrm{M}},V_{\mathrm{B}}}(\boldsymbol{q},t) = N\langle \Delta C_{\mathrm{b,b}}^{V_{\mathrm{m}},V_{\mathrm{B}}}(\boldsymbol{q},t)\rangle_N = N\Delta C_{\mathrm{b,b}}^{V_{\mathrm{m}},V_{\mathrm{B}}}(q) \tag{23}$$

which again removes the dependence on orientation and time.

Although the choice of V_{m} may appear arbitrary, it introduces no ambiguity in the computed intensity. Expanding or contracting V_{m} merely shifts contributions between the molecular, buffer, and cross-terms in Eq. 18, but leaves their *sum*—the total measured intensity—unchanged. This freedom of choosing V_{m} is used advantageously in Sec. IV, where the bulk contribution is shown to cancel under background subtraction.

5. Combining everything: the observable scattering

We now have all the components required to assemble the observable solution scattering intensity. Starting from Eq. 18 and applying the results of Eqs. 20, 21, 22, and

23:

$$I_s(q) = \Delta I_M(\boldsymbol{q},t) + \Delta I_b^{(V_B)}(\boldsymbol{q},t) + \Delta C_{M,b}^{V_M,V_B}(\boldsymbol{q},t)$$
$$= \underbrace{N\Delta I_m^*(q)}_{\text{molecular term}} + \underbrace{\Delta I_b^{(V_b)}(q) + N\Delta C_{b,b}^{V_m,V_B}(q)}_{\text{buffer terms}} \quad (24)$$

Eq. 24 is the central result of our derivations until now. It expresses the observable intensity as a sum of three physically meaningful components: (i) excess scattering from the molecules, including nearby structured solvent, (ii) excess scattering from pure buffer, and (iii) excess scattering from short-range buffer–buffer correlations across the interfacial region. This decomposition makes explicit which parts of the signal originate from the molecule of interest and which arise from its solvent environment.

With this analytical framework established, the remainder of this paper examines how it can be applied to interpret and model experimentally measured scattering intensities.

IV. BACKGROUND SUBTRACTION

In a typical SAS measurement, the recorded intensity $I_s(q)$ is overwhelmingly dominated by buffer contributions, obscuring the structural information of interest. The standard remedy is to record a second measurement of buffer alone and subtract it from the first. In this section, we examine how this subtraction is formalized and what assumptions it requires.

A. The necessity of background subtraction

The objective of background subtraction is to remove the excess buffer terms from the observable intensity (Eq. 24). To achieve this, we consider two systems measured under similar experimental conditions (Fig. 12):

System A: Sample in buffer. *System B*: Buffer only.

The corresponding measured intensities are:

$$I_A^{(\text{exp})}(q) \equiv I_s(q) \qquad I_B^{(\text{exp})}(q) \equiv I_b^{(V_S)}(q) = \Delta I_b^{(V_S)}(q) \quad (25)$$

where the uniform background density ρ_b contributes only to the (unobserved) forward scattering and is therefore omitted (see Sec. III.A). Using these two measured intensities, two subtraction schemes are commonly employed: *direct subtraction* and *volume-corrected subtraction*, differing only in their treatment of the cross-term.

1. Scheme 1: Direct subtraction

Inspired by the approach of Park *et al.* (2009), we apply to system B the same volume partitioning used for system A. Because system B contains no molecule, the molecular partition V_m is filled with bulk buffer, and Eq. 24 reduces to:

$$I_B^{(\text{exp})}(q) = N\Delta I_b^{(V_m)}(q) + \Delta I_b^{(V_B)}(q) + N\Delta C_{b,b}^{V_m,V_B}(q) \quad (26)$$

Because both systems use the same boundary, both their bulk and cross-terms are identical; see Fig. 13. Upon *direct* subtraction, they therefore cancel:

$$I_A^{(\text{exp})}(q) - I_B^{(\text{exp})}(q)$$
$$= \left\{N\Delta I_m^*(q) + \Delta I_b^{(V_B)}(q) + N\Delta C_{b,b}^{V_m,V_B}(q)\right\}$$
$$- \left\{N\Delta I_b^{(V_m)}(q) + \Delta I_b^{(V_B)}(q) + N\Delta C_{b,b}^{V_m,V_B}(q)\right\}$$
$$= N\left[\Delta I_m^*(q) - \Delta I_b^{(V_m)}(q)\right] \quad (27)$$

Though this subtraction scheme does not fully isolate the molecular scattering, the remaining buffer contribution has been reduced to a volume V_m of bulk buffer. This is a significant reduction: the *residual* contribution $\Delta I_b^{(V_m)}(q)$ is purely a bulk quantity, independent of the molecule, and can in principle be computed once and for all—for instance, from MD simulations of pure solvent (Sec. VI.D). Given such a computation, the residual can be subtracted, and the direct subtraction scheme recovers the molecular intensity exactly.

2. Scheme 2: Volume-corrected subtraction

To avoid explicit evaluation of the residual buffer term $\Delta I_b^{(V_m)}(q)$ in Eq. 27, a practical approximation neglects the cross-term in Eq. 26; this is justified for molecules with a small surface-to-volume ratio (App. A1.2). The residual buffer contribution then reduces to:

$$N\Delta I_b^{(V_m)}(q) \approx \Delta I_b^{(V_S)}(q) - \Delta I_b^{(V_B)}(q) \quad (28)$$

Since $V_M = V_S - V_B$, this approximation makes buffer scattering proportional to buffer volume. Introducing the excess buffer intensity per unit volume $\Delta\hat{I}_b(q) \equiv \Delta I_b^{(V_S)}(q)/V_S$, so that $\Delta I_b^{(V)}(q) = V\Delta\hat{I}_b(q)$ for any buffer volume V, we can re-express the residual buffer term in Eq. 27 as:

$$N\Delta I_b^{(V_m)}(q) = NV_m\Delta\hat{I}_b(q) = \nu V_S\Delta\hat{I}_b(q) = \nu I_B^{(\text{exp})}(q)$$

where $\nu \equiv NV_m/V_S$ is the molecular volume fraction.[7] Substituting back into Eq. 27 and rearranging yields the

[7] Beware that this is the volume fraction of the *modeling* volume V_m, which is substantially larger than the *physical* molecular volume V_m'.

FIG. 12 Visualization of the two background subtraction schemes. The left side shows how the measured system intensities may be interpreted in terms of excess densities, obtained by rescaling the measured densities using Babinet's principle (Sec. III.A.2). The right side illustrates two common conventions for background subtraction using the intensities from Systems A and B, used to isolate the scattering signal from the molecules. This schematic form understates the substantial theoretical derivations underlying the relations.

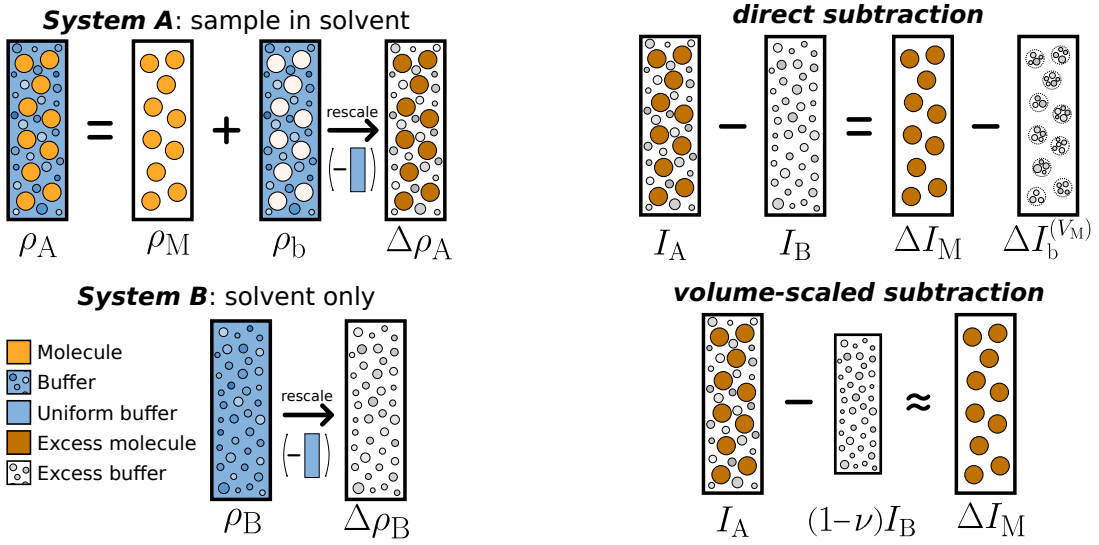
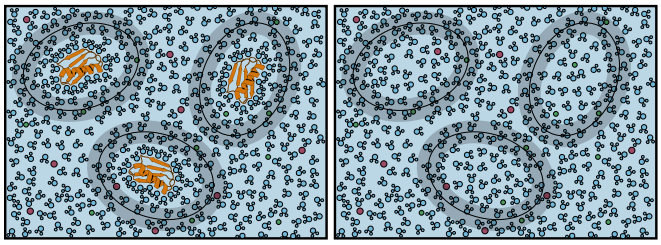


FIG. 13 Illustration of cross-term cancellation. Partitioning system B (right) into the same regions as system A (left) ensures that cross-correlations across identical boundaries cancel upon subtraction. Because this partitioning is arbitrary, the final observable cannot depend on its shape or size.



volume-corrected subtraction:

$$I_{\mathrm{A}}^{(\mathrm{exp})}(q) - (1-\nu) I_{\mathrm{B}}^{(\mathrm{exp})}(q) \approx N \Delta I_{\mathrm{m}}^{*}(q)$$

This approximation is attractive because it removes the need to model bulk solvent: after volume-scaled subtraction, only the molecular contribution remains. However, as it relies on neglecting boundary cross-terms, the associated error scales with interfacial area and becomes significant for smaller molecules with their larger surface-to-volume ratio or at wider angles where buffer contributions dominate (App. A1.2).

B. Practical implications for SAS analysis

To recap, two background subtraction schemes are used in practice:

$$I_{\mathrm{A}}^{(\mathrm{exp})}(q) - I_{\mathrm{B}}^{(\mathrm{exp})}(q) \qquad \text{(direct)}$$
$$I_{\mathrm{A}}^{(\mathrm{exp})}(q) - (1-\nu) I_{\mathrm{B}}^{(\mathrm{exp})}(q) \qquad \text{(volume-corrected)}$$

Although the two schemes appear similar, they make fundamentally different assumptions about how the buffer contributes, and this distinction determines when each scheme is appropriate.

When the residual buffer term $\Delta I_b^{(V_m)}(q)$ *can be evaluated*—e.g. through molecular dynamics simulations (Sec. VI.D)—the direct subtraction scheme is exact; any remaining error depends on the residual computation, not on the subtraction itself.

When the residual buffer term cannot be computed, the volume-corrected scheme provides a practical alternative; its approximation error arises from neglecting boundary cross-terms and therefore scales with interfacial area, making it reliable for larger solutes but inaccurate for small particles and at wider scattering angles (App. A1.2).

These derivations demonstrate that background subtraction is not merely a step in the experimental pipeline, but an integral component of the theoretical model. Thus, SAS analysis programs must assume a convention. MD-oriented programs insvolving explicit, all-atom

solvent models typically assume direct subtraction. In contrast, more conventional programs do not model the residual buffer term $\Delta I_{\mathrm{b}}^{(V_{\mathrm{m}})}(q)$ and are, therefore, only consistent with the volume-corrected scheme. Using a different scheme than the one assumed by the analysis software introduces systematic errors that are difficult to diagnose. The recommended strategy is therefore to let the analysis software perform the subtraction, ensuring consistency with its internal modeling assumptions.

1. Accounting for instrumental scattering

Before closing this chapter, we briefly address contributions from the system container and instrument, which we have so far ignored. Under direct subtraction, these contributions cancel provided both measurements share identical geometry and normalization. In contrast, they typically do not cancel under the volume-corrected scheme due to the $(1-\nu)$ scaling factor, requiring explicit correction procedures (Pauw *et al.*, 2017). Other effects, such as beam smearing, resolution limitations, and finite coherence lengths, are beyond the scope of this work; for a detailed discussion, see Pedersen *et al.* (1990) and Shinohara and Amemiya (2015).

V. MODELING WITHOUT ATOMISTIC STRUCTURES

With the theoretical foundations in place, we now turn to practical applications. This section focuses on strategies for interpreting scattering data with little to no prior structural knowledge, whereas Sec. VI addresses validation and refinement when atomistic structures are available. Readers interested primarily in structure-based approaches may refer directly to Sec. VI.

In many experimental scenarios, atomistic models are either unknown or unreliable. How, then, can we extract meaningful structural insights directly from an observed scattering profile? To address this question, we explore a spectrum of strategies: model-independent methods that reveal global shape information, analytical scattering models for idealized geometries, and numerical approaches for complex or irregular structures. For each, we examine the underlying principles, highlight their strengths and limitations, and outline practical considerations for application.

Throughout this chapter, we base our analysis on the representative molecular density $\Delta\rho_{\mathrm{m}}^{*}(\boldsymbol{r})$ and rely on Eqs. 7 and 8 to relate these results to the total system intensity.

A. Model-independent analysis

We begin with examining what model-independent information may be extracted directly from the scattering profile, without invoking any structural assumptions.

1. Guinier approximation

André Guinier (Guinier, 1939; Guinier *et al.*, 1956) demonstrated that the low-q limit of the scattering intensity contains information on overall molecular shape and size. To obtain this result, the Taylor expansion of the sinc term in the Debye equation (Eq. 10) is used for small q:

$$\operatorname{sinc} x = 1 - \frac{x^2}{6} + O\left(x^4\right),$$

where terms of order $O(x^4)$ or higher are neglected. For brevity, we suppress the q-dependence of all form factors.

Expanding the Debye equation:

$$\begin{aligned} I_{\mathrm{m}}^{*}(q) &= \sum_{ij} f_i f_j \operatorname{sinc} q r_{ij} \\ &\approx \sum_{ij} f_i f_j \left(1 - \frac{(q r_{ij})^2}{6} + O\left(q^4\right)\right) \end{aligned} \tag{29}$$

The pairwise distance is:

$$r_{ij}^2 = |\boldsymbol{r}_i - \boldsymbol{r}_j|^2 = r_i^2 + r_j^2 - 2\boldsymbol{r}_i \cdot \boldsymbol{r}_j \tag{30}$$

We place the origin of our coordinate system at the electron-weighted center of mass, such that:

$$\sum_i f_i \, \boldsymbol{r}_i = \mathbf{0}$$

Substituting Eq. 30 into Eq. 29:

$$I_{\mathrm{m}}^{*}(q) = \sum_{ij} f_i f_j - \frac{q^2}{6} \sum_{ij} f_i f_j \left(r_i^2 + r_j^2 - 2\boldsymbol{r}_i \cdot \boldsymbol{r}_j\right)$$

The sums involving r_i^2 and r_j^2 are identical upon relabeling the indices, and may be combined:

$$\begin{aligned} I_{\mathrm{m}}^{*}(q) = \Big(\sum_i f_i\Big)^2 - \frac{q^2}{3} \sum_{ij} f_i f_j r_i^2 \\ + \frac{q^2}{3} \sum_i \Big[f_i \boldsymbol{r}_i \cdot \underbrace{\Big(\sum_j f_j \boldsymbol{r}_j\Big)}_{\mathbf{0}}\Big] \end{aligned}$$

The third term vanished by our choice of origin, leaving

only:

$$\begin{aligned} I^*_{\mathrm{m}}(q) &= \left(\sum_i f_i\right)^2 - \frac{q^2}{3}\sum_i f_i r_i^2 \sum_j f_j \\ &= \left(\sum_i f_i\right)^2 \left\{1 - \frac{q^2}{3}\frac{\sum_i f_i r_i^2}{\sum_i f_i}\right\} \\ &\approx I^*_{\mathrm{m}}(0)\exp\left(-\frac{q^2 R_g^2}{3}\right) \end{aligned}$$

where the exponential form follows by re-exponentiating to the same order in q^2, and $R_g^2 = \sum_i f_i r_i^2 \,/\, \sum_i f_i$ is the electron-weighted radius of gyration.[8] This result is consistent with our discussion in App. A2: at small q, scattering is dominated by lower-order spherical harmonics, capturing only overall shape and size.

2. Porod asymptotic

At the opposite end of the angular range, the high-q regime provides insight into fine structural details. Porod showed that, for particles with sharp interfaces, the scattering intensity decays with a q^{-4} power law reflecting interfacial surface area. The full derivation requires asymptotic analysis of Fourier transforms across discontinuities, which lies outside the framework developed here; we refer the reader to Ciccariello *et al.* (2002) for a comprehensive treatment and state only the result.

Assuming a well-defined boundary between phases and taking the limit $q \to \infty$, Porod obtained (Porod, 1951, 1953):

$$\lim_{q\to\infty} I(q) = \frac{2\pi\Delta\rho_{\mathrm{m}}^2}{q^4} S_{\mathrm{int}}$$

where S_{int} is the interfacial surface area between the phases. This result applies universally whenever a distinct interface exists, regardless of molecular concentration.

Deviations from the expected q^{-4} scaling can reveal additional structural features such as surface roughness, fractal geometry, or a gradual phase transition rather than sharp boundaries (Svergun *et al.*, 2013).

[8] Note that the sum runs over *all* atoms, including the hydration shell, in the modeling volume V_{m}; the extracted R_g is therefore the hydrated radius of gyration. This applies to all results derived in this section.

3. Pair-distance distribution

The pair-distance distribution function provides some of the most detailed model-independent real-space information obtainable from SAS. It describes the probability-weighted distribution of distances between all pairs of points within the molecule, and establishes a direct link between the measured intensity and the spatial structure.

Starting from the definition of excess molecular intensity:

$$\begin{aligned} \Delta I^*_{\mathrm{m}}(q) &= \langle |\Delta A^*_{\mathrm{m}}(\boldsymbol{q})|^2 \rangle_\Omega \\ &= \left\langle \int_{V_{\mathrm{m}}} \Delta\rho^*_{\mathrm{m}}(\boldsymbol{r}_1) e^{i\boldsymbol{q}\cdot\boldsymbol{r}_1} d\boldsymbol{r}_1 \int_{V_{\mathrm{m}}} \Delta\rho^*_{\mathrm{m}}(\boldsymbol{r}_2) e^{-i\boldsymbol{q}\cdot\boldsymbol{r}_2} d\boldsymbol{r}_2 \right\rangle_\Omega \\ &= \left\langle \iint_{V_{\mathrm{m}}} \Delta\rho^*_{\mathrm{m}}(\boldsymbol{r}_1)\Delta\rho^*_{\mathrm{m}}(\boldsymbol{r}_2) e^{i\boldsymbol{q}\cdot(\boldsymbol{r}_1-\boldsymbol{r}_2)} d\boldsymbol{r}_1 d\boldsymbol{r}_2 \right\rangle_\Omega \end{aligned}$$

With the change of variables $\boldsymbol{r} = \boldsymbol{r}_1 - \boldsymbol{r}_2$ and $\boldsymbol{r}' = \boldsymbol{r}_2$:

$$\begin{aligned} \Delta I^*_{\mathrm{m}}(q) &= \left\langle \iint_{V_{\mathrm{m}}} \Delta\rho^*_{\mathrm{m}}(\boldsymbol{r}+\boldsymbol{r}')\Delta\rho^*_{\mathrm{m}}(\boldsymbol{r}') e^{i\boldsymbol{q}\cdot\boldsymbol{r}} d\boldsymbol{r} d\boldsymbol{r}' \right\rangle_\Omega \\ &= \left\langle \int_{V_{\mathrm{m}}} e^{i\boldsymbol{q}\cdot\boldsymbol{r}} \int_{V_{\mathrm{m}}} \Delta\rho^*_{\mathrm{m}}(\boldsymbol{r}+\boldsymbol{r}')\Delta\rho^*_{\mathrm{m}}(\boldsymbol{r}') d\boldsymbol{r}' d\boldsymbol{r} \right\rangle_\Omega \end{aligned}$$

The inner integral is recognized as the *correlation* function of the excess density:

$$\Delta\gamma^*_{\mathrm{m}}(\boldsymbol{r}) \equiv \int_{V_{\mathrm{m}}} \Delta\rho^*_{\mathrm{m}}(\boldsymbol{r}+\boldsymbol{r}')\Delta\rho^*_{\mathrm{m}}(\boldsymbol{r}') d\boldsymbol{r}'$$

This correlation function, originally introduced by Debye and Bueche (1949), describes how density variations at $\boldsymbol{r}'$ correlate with those at $\boldsymbol{r}$. Substituting this into the integral:

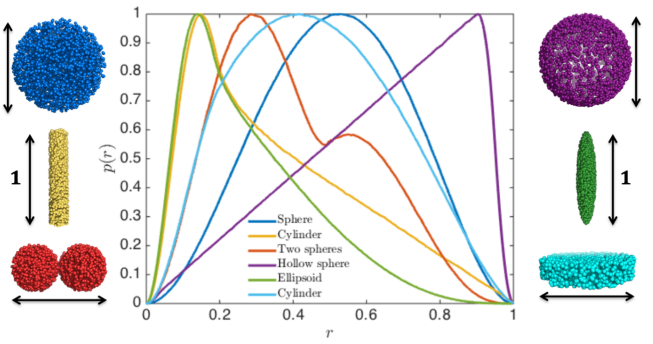
$$\Delta I^*_{\mathrm{m}}(q) = \left\langle \int_{V_{\mathrm{m}}} \Delta\gamma^*_{\mathrm{m}}(\boldsymbol{r}) e^{i\boldsymbol{q}\cdot\boldsymbol{r}} d\boldsymbol{r} \right\rangle_\Omega$$

There is no general analytic solution for the orientational average because the correlation function and phase factor are coupled. To proceed, recall that $\Delta\rho^*_{\mathrm{m}}(\boldsymbol{r})$ is itself a representative density: it stands in for an ensemble of molecular orientations sampled in solution (Sec. II.D.2). The correlation function $\Delta\gamma^*_{\mathrm{m}}(\boldsymbol{r})$ inherits this average and, by isotropy of the solution, is rotationally symmetric, $\Delta\gamma^*_{\mathrm{m}}(\boldsymbol{r}) = \Delta\gamma^*_{\mathrm{m}}(r)$. The orientational average is:

$$\begin{aligned} \Delta I^*_{\mathrm{m}}(q) &= \int_{V_{\mathrm{m}}} \Delta\gamma^*_{\mathrm{m}}(r)\langle e^{i\boldsymbol{q}\cdot\boldsymbol{r}}\rangle_\Omega d\boldsymbol{r} \\ &= \int_0^\infty 4\pi r^2 \Delta\gamma^*_{\mathrm{m}}(r)\,\mathrm{sinc}\,qr\,dr \\ &= \int_0^\infty \Delta p^*_{\mathrm{m}}(r)\,\mathrm{sinc}\,qr\,dr \end{aligned} \tag{31}$$

where we have defined the pair distance distribution function $\Delta p^*_{\mathrm{m}}(r) \equiv 4\pi r^2 \Delta\gamma^*_{\mathrm{m}}(r)$.

FIG. 14 The pair distance distribution function for different shapes, normalized along their longest dimension. Reprinted with permission from Larsen (2018).



Eq. 31 shows that the intensity is given as the Fourier sine transform of $\Delta p^*_{\mathrm{m}}(r)$. In principle, we can therefore recover Δp^*_{m} from the intensity through the inverse transform:

$$q\Delta I^*_{\mathrm{m}}(q) = \int_0^\infty \frac{\Delta p^*_{\mathrm{m}}(r)}{r} \sin qr\, dr$$
$$\frac{\Delta p^*_{\mathrm{m}}(r)}{r} = \frac{2}{\pi}\int_0^\infty q\Delta I^*_{\mathrm{m}}(q) \sin qr\, dq$$

In practice, this inversion is ill-posed due to the limited measurable q-range and experimental noise. Stabilized indirect Fourier transform methods are therefore employed practically; see Glatter (1977) or Svergun *et al.* (2013) for details.

Once $\Delta p^*_{\mathrm{m}}(r)$ is obtained, the maximum molecular dimension $D_{\max}$ is estimated as the distance where $\Delta p^*_{\mathrm{m}}(r)$ vanishes. This is illustrated by $\Delta p^*_{\mathrm{m}}(r)$ curves for several shapes in Fig. 14, from which not only the maximum extent may be estimated, but also other characteristic distances of the shape. As an example, the thicknesses of the two elongated shapes may be estimated as their most frequent distance (14, yellow and green).

B. Analytical scattering models

Many systems of interest have well-characterized overall geometry—globular proteins, spherical micelles, rod-like assemblies—even when their internal structure is not. In such cases, the scattering can be derived analytically by assuming a simple geometric form for $\Delta\rho^*_{\mathrm{m}}(\boldsymbol{r})$ and evaluating the amplitude integral in closed form. The resulting expressions provide low-resolution scattering models that can be fitted to experimental data, allowing rapid shape characterization. We derive intensities for a few geometric cases below; for a comprehensive catalogue, see Pedersen, J.S. in Lindner and Oberdisse (2024).

Analytical shape models predict the scattering signal according to the volume-corrected background subtraction scheme, $I_{\mathrm{A}}^{(\mathrm{exp})}(q) - (1-\nu) I_{\mathrm{B}}^{(\mathrm{exp})}(q) \approx N\Delta I^*_{\mathrm{m}}(q)$, which requires only the single-molecule term $\Delta I^*_{\mathrm{m}}(q)$ to be modeled. The approximation holds at small q, where the neglected boundary cross-term and hydration-shell contributions are small; fitting at wider q, or to directly-subtracted data, mixes the model intensity with unmodeled buffer terms and yields biased structural parameters.

1. Homogeneous spheres

The molecular density of a homogeneous sphere is defined as:

$$\Delta\rho^*_{\mathrm{m}}(\boldsymbol{r}) = \begin{cases} \Delta\rho_{\mathrm{c}} & \text{if } r < R \\ 0 & \text{otherwise} \end{cases}$$

The associated scattering amplitude is:

$$\begin{aligned}
\Delta A^*_{\mathrm{m}}(\boldsymbol{q}) &= \int_V \Delta\rho^*_{\mathrm{m}}(\boldsymbol{r}) e^{i\boldsymbol{q}\cdot\boldsymbol{r}} d\boldsymbol{r} \\
&= \Delta\rho_{\mathrm{c}} \int_0^R dr \int_0^\pi d\phi \int_0^{2\pi} e^{iqr\cos\theta} r^2 \sin\theta\, d\theta \\
&= \Delta\rho_{\mathrm{c}}(2\pi) \int_0^R \frac{2r\sin qr}{q} dr \\
&= \Delta\rho_{\mathrm{c}} \frac{4\pi}{3}\left[3\frac{\sin qR - qR\cos qR}{q^3}\right] \\
&= \Delta\rho_{\mathrm{c}} V_{\mathrm{sphere}} \left[3\frac{j_1(qR)}{qR}\right]
\end{aligned} \tag{32}$$

where $j_1(x) = (\sin x - x\cos x)/x^2$ is the spherical Bessel function. The intensity is obtained by squaring this amplitude; no orientational averaging is needed due to spherical symmetry.

2. Fitting analytical models to experimental data

Analytical shape models are compared with experimental data by fitting their free parameters—e.g. $\Delta\rho_{\mathrm{c}}$ and R for the homogeneous sphere. In practice, tools such as SasView (Adams *et al.*, 2024) introduce additional adjustable parameters to account for experimental factors not captured by the shape model alone: the number of molecules N is absorbed into an overall scaling factor a, an additive constant b corrects for any uniform background, and the bulk solvent density ρ_{b} may be used as a free parameter in addition to ρ_{c}. The resulting model intensity for the homogeneous sphere then takes the form:

$$\begin{aligned}
\Delta I^{(\mathrm{model})}_{\mathrm{m}}(q) &= a\Delta I^*_{\mathrm{m}}(q) + b \\
&= a(\rho_{\mathrm{c}} - \rho_{\mathrm{b}})^2 \left(\frac{4\pi R^3}{3}\right)^2 \left[3\frac{j_1(qR)}{qR}\right]^2 + b
\end{aligned}$$

To reduce the risk of overfitting, free parameters can be constrained with independent information; this is especially important for more complex models with many such parameters.

A similar strategy applies to interparticle correlations: when intermolecular interactions are significant, the structure factor $S(q)$ may be parameterized in an analogous way and fitted simultaneously with the shape model to account for concentration-dependent scattering; see Larsen *et al.* (2020).

3. Core–shell structures

The core–shell model is widely used to describe micelles, vesicles, and nanoparticles with distinct internal and external regions of homogeneous density. The molecular excess density is:

$$\Delta\rho_{\mathrm{m}}^{*}(\boldsymbol{r}) = \begin{cases} \Delta\rho_{\mathrm{c}} & \text{if } r < R_{\mathrm{C}} \\ \Delta\rho_{\mathrm{s}} & \text{if } R_{\mathrm{C}} < r < R_{\mathrm{S}} \\ 0 & \text{otherwise} \end{cases}$$

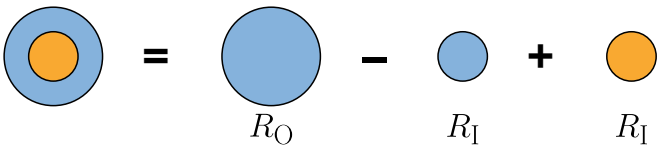
Denoting by V_{C} and V_{S} the volumes enclosed by R_{C} and R_{S}, the corresponding scattering amplitude is:

$$\begin{aligned} \Delta A_{\mathrm{m}}^{*}(\boldsymbol{q}) &= \int_{V_{\mathrm{C}}} \Delta\rho_{\mathrm{c}} e^{i\boldsymbol{q}\cdot\boldsymbol{r}} d\boldsymbol{r} + \int_{V_{\mathrm{S}}-V_{\mathrm{C}}} \Delta\rho_{\mathrm{s}} e^{i\boldsymbol{q}\cdot\boldsymbol{r}} d\boldsymbol{r} \\ &= \int_{V_{\mathrm{C}}} \Delta\rho_{\mathrm{c}} e^{i\boldsymbol{q}\cdot\boldsymbol{r}} d\boldsymbol{r} + \int_{V_{\mathrm{S}}} \Delta\rho_{\mathrm{s}} e^{i\boldsymbol{q}\cdot\boldsymbol{r}} d\boldsymbol{r} - \int_{V_{\mathrm{C}}} \Delta\rho_{\mathrm{s}} e^{i\boldsymbol{q}\cdot\boldsymbol{r}} d\boldsymbol{r} \\ &= \int_{V_{\mathrm{C}}} (\Delta\rho_{\mathrm{c}} - \Delta\rho_{\mathrm{s}}) e^{i\boldsymbol{q}\cdot\boldsymbol{r}} d\boldsymbol{r} + \int_{V_{\mathrm{S}}} \Delta\rho_{\mathrm{s}} e^{i\boldsymbol{q}\cdot\boldsymbol{r}} d\boldsymbol{r} \\ &= 3\left[(\Delta\rho_{\mathrm{c}} - \Delta\rho_{\mathrm{s}})\, V_{\mathrm{C}} \frac{j_1(qR_{\mathrm{C}})}{qR_{\mathrm{C}}} + \Delta\rho_{\mathrm{s}} V_{\mathrm{S}} \frac{j_1(qR_{\mathrm{S}})}{qR_{\mathrm{S}}}\right] \end{aligned} \tag{33}$$

where we have used the result of Sec. V.B.1, $V_{\mathrm{C}} = 4\pi R_{\mathrm{C}}^3/3$, and $V_{\mathrm{S}} = 4\pi R_{\mathrm{S}}^3/3$. This expression reduces to the amplitude of a homogeneous sphere for $\Delta\rho_{\mathrm{s}} = 0$.

Eq. 33 may also be interpreted as the sum of three spherical components—a sphere of volume V_{S} with density $\Delta\rho_{\mathrm{s}}$, and two spheres of volume V_{C} with densities $\Delta\rho_{\mathrm{c}}$ and $-\Delta\rho_{\mathrm{s}}$—as illustrated in Fig. 15. Such decompositions are helpful and follow from the linearity of the Fourier transform. For intensities, in contrast, such decompositions are not valid since squaring the amplitude leads to cross-terms that generally do not vanish.

FIG. 15 Illustration of how the total amplitude for a core–shell molecule is constructed from summing component amplitudes, leveraging the linearity of the Fourier transform.



4. Gaussian chains

We now turn to a more complex model: the *Gaussian chain*, a simple model of polymers in solution. This model represents a flexible chain of N scatterers connected by segments whose orientations are random and uncorrelated.

Using Eq. 5, the molecular amplitude is given by $\Delta A_{\mathrm{m}}^{*}(\boldsymbol{q}) = \sum_i^N \Delta f_i(\boldsymbol{q}) e^{i\boldsymbol{q}\cdot\boldsymbol{r}_i}$, where $\Delta f_i(\boldsymbol{q})$ is an excess form factor. By restricting our analysis to identical spherical scatterers, such as atoms, these are orientationally independent: $\Delta f_i(\boldsymbol{q}) = \Delta f(q)$. The associated intensity for a chain with N segments is then:

$$\begin{aligned} \Delta I_{\mathrm{m}}^{*}(q) &= \langle |\Delta A_{\mathrm{m}}^{*}(\boldsymbol{q})|^2 \rangle_\Omega \\ &= \Delta f^2(q) \sum_{i,j=1}^{N} \left\langle e^{i\boldsymbol{q}\cdot(\boldsymbol{r}_i - \boldsymbol{r}_j)} \right\rangle_\Omega \end{aligned}$$

where $\boldsymbol{r}_i - \boldsymbol{r}_j$ is the vector connecting scatterers i and j. Evaluating this expression requires a closer look at the chain statistics.

The position of the ith scatterer is given as the vector sum of offsets relative to the first:

$$\boldsymbol{r}_i = \boldsymbol{r}_0 + \sum_{k=1}^{i} \delta\boldsymbol{r}_k$$

where the segment vectors $\delta\boldsymbol{r}_k$ are assumed independent and Gaussian-distributed with zero mean, $\langle \delta\boldsymbol{r}_k \rangle = 0$, and variance $\langle \delta\boldsymbol{r}_k^2 \rangle = l_0^2$. Assuming $i > j$, the separation between two scatterers is:

$$\boldsymbol{r}_i - \boldsymbol{r}_j = \sum_{k=j+1}^{i} \delta\boldsymbol{r}_k$$

and the mean squared displacement between them is:

$$\begin{aligned} \langle (\boldsymbol{r}_i - \boldsymbol{r}_j)^2 \rangle_\Omega &= \left\langle \Big(\sum_{k=j+1}^{i} \delta\boldsymbol{r}_k \Big) \cdot \Big(\sum_{l=j+1}^{i} \delta\boldsymbol{r}_l \Big) \right\rangle_\Omega \\ &= \sum_{k=j+1}^{i} \langle (\delta\boldsymbol{r}_k)^2 \rangle_\Omega + 2 \sum_{k=j+1}^{i} \sum_{l=k+1}^{i} \langle \delta\boldsymbol{r}_k \cdot \delta\boldsymbol{r}_l \rangle_\Omega \end{aligned}$$

The second term vanishes due to independence: $\langle \delta \boldsymbol{r}_k \cdot \delta \boldsymbol{r}_l \rangle_\Omega = \langle \delta \boldsymbol{r}_k \rangle_\Omega \langle \delta \boldsymbol{r}_l \rangle_\Omega = 0$. The remaining term is:

$$\begin{aligned}\langle (\boldsymbol{r}_i - \boldsymbol{r}_j)^2 \rangle_\Omega &= l_0^2 \sum_{k=j+1}^{i} 1 \\ &= l_0^2 |i-j|\end{aligned}$$

This mean squared displacement determines the orientational average in the intensity expression. A standard result for sums of independent Gaussian vectors gives (Isserlis, 1918):

$$\left\langle e^{i\boldsymbol{q}\cdot(\boldsymbol{r}_i - \boldsymbol{r}_j)} \right\rangle_\Omega = e^{-q^2 \langle (\boldsymbol{r}_i - \boldsymbol{r}_j)^2 \rangle_\Omega / 6} = e^{-q^2 l_0^2 |i-j|/6}$$

As the full derivation is somewhat technical, we use this result here without proof. Substituting back into the intensity gives:

$$\Delta I_\mathrm{m}^*(q) = \Delta f^2(q) \sum_{i,j=1}^{N} e^{-q^2 l_0^2 |i-j|/6}$$

For long chains, $|i-j|$ can be considered continuous, allowing us to replace the sum by an integral:

$$\begin{aligned}\Delta I_\mathrm{m}^*(q) &= \Delta f^2(q) \int_0^N \int_0^N e^{-q^2 l_0^2 |n-n'|/6} dn' dn \\ &= 2\Delta f^2(q) \int_0^N \int_0^n e^{-q^2 l_0^2 (n-n')/6} dn' dn \\ &= 2\Delta f^2(q) \int_0^N 6 \frac{1 - e^{-q^2 l_0^2 n/6}}{q^2 l_0^2} dn \\ &= 2\Delta f^2(q) 6 \frac{6e^{-q^2 l_0^2 N/6} + Nq^2 l_0^2 - 6}{q^4 l_0^4}\end{aligned}$$

Defining $x = Nq^2 l_0^2/6$, this result takes the simple form:

$$\Delta I_\mathrm{m}^*(q) = 2N^2 \Delta f^2(q) \frac{e^{-x} + x - 1}{x^2} \tag{34}$$

This result, first derived by Debye (1947), is known as the *Debye function* for Gaussian chains.[9] At low q, it reduces to the Guinier approximation with $R_g^2 = Nl_0^2/6$, while at high q it exhibits a q^{-2} decay characteristic of flexible polymers.

Other statistical models include star polymers (Benoit, 1953), ring polymers (Zimm and Stockmayer, 1949), and variants incorporating self-avoidance ("excluded volume") (Li *et al.*, 2014; Pedersen and Schurtenberger, 1996); see (Lindner and Oberdisse, 2024; Pedersen, 1997; Svaneborg and Pedersen, 2012) for comprehensive reviews. Despite these advancements, complex statistical models can rarely be solved analytically, and often require empirical parameterization of simulated results (Pedersen and Schurtenberger, 1996).

[9] The factor N^2 is typically absorbed into an overall scaling factor in the literature.

C. Numerical scattering calculations

The analytical results above cover shapes with enough symmetry to admit closed-form solutions. For more complex geometries—branched structures, disordered assemblies, or atomistic models—closed-form expressions are typically not available and the intensity must be computed numerically. We outline three widely used approaches in this section.

1. Monte Carlo sampling of the amplitude integral

When the structure is too complex to admit a closed-form expression, Monte Carlo integration offers a numerical alternative for evaluating the amplitude integral (Caflisch, 1998; Hansen, 1990; Hung, 2024; Pedersen *et al.*, 2012). Starting from the molecular scattering amplitude:

$$\Delta A_\mathrm{m}^*(\boldsymbol{q}) = \int_{V_\mathrm{m}} \Delta \rho_\mathrm{m}^*(\boldsymbol{r}) e^{i\boldsymbol{q}\cdot\boldsymbol{r}} d\boldsymbol{r}$$

This integral can be approximated by uniformly sampling N points from V_m and averaging:

$$\Delta A_\mathrm{m}^*(\boldsymbol{q}) \approx \frac{V_\mathrm{m}}{N} \sum_i^N \Delta \rho_\mathrm{m}^*(\boldsymbol{r}_i) e^{i\boldsymbol{q}\cdot\boldsymbol{r}_i}$$

where the N points $\{\boldsymbol{r}_i\}$ are assumed to be uniformly sampled from V_m for simplicity. More sophisticated strategies, such as importance sampling, can improve computational efficiency (Hung, 2024).

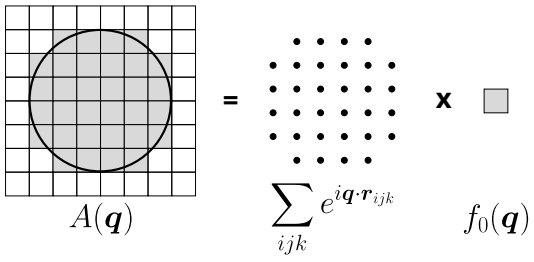
Squaring and orientationally averaging to obtain the intensity:

$$\begin{aligned}\Delta I_\mathrm{m}^*(q) &= \langle |\Delta A_\mathrm{m}^*(\boldsymbol{q})|^2 \rangle_\Omega \\ &= \left(\frac{V_\mathrm{m}}{N}\right)^2 \sum_{ij}^N \Delta \rho_\mathrm{m}^*(\boldsymbol{r}_i) \Delta \rho_\mathrm{m}^*(\boldsymbol{r}_j) \operatorname{sinc}(q r_{ij})\end{aligned}$$

This approach has been implemented in several SAS analysis tools (Deumer *et al.*, 2022; Hansen, 1990; Larsen *et al.*, 2023; Pedersen *et al.*, 2012; Spinozzi *et al.*, 2000), where it is used for validating analytic results or for handling complex geometries.

Although this expression resembles the Debye equation for point scatterers, and some derivations indeed begin from there, the resemblance is superficial: the points $\{\boldsymbol{r}_i\}$ are quadrature nodes, not physical scatterers, and the factor V_m/N is an integration weight, not a structural property. The underlying object is the continuous volume integral above, recovered as $N \to \infty$.

FIG. 16 Illustration of the grid decomposition of a homogeneous sphere. The scattering amplitude factors into a form factor term (cell shape) and a geometrical term (cell positions).



2. Representing arbitrary shapes with a grid

To evaluate the scattering of an arbitrary shape or object, instead of summing over its atoms, it can be convenient to partition the scattering volume into a three-dimensional grid of cells indexed by i, j, k. The density is then given as:

$$\rho^*_{\mathrm{m}}(\boldsymbol{r}) = \sum_{ijk} \rho(\boldsymbol{r} - \boldsymbol{r}_{ijk})$$

where we use an absolute density as this technique is mostly useful for evaluating uniform densities. Following the same steps used to derive the sum-over-scatterers amplitude in Sec. II.C.1, we obtain:

$$A^*_{\mathrm{m}}(\boldsymbol{q}) = \sum_{ijk} e^{i\boldsymbol{q}\cdot\boldsymbol{r}_{ijk}} f_{ijk}(\boldsymbol{q})$$

This expression closely matches the aforementioned sum-of-scatterers amplitude (Eq. 5): in the grid-based formulation, each cell acts as an independent scattering center.

As a practical example, consider a homogeneous solid particle of density ρ_0. Representing it using a regular cubic grid as in Fig. 16, all interior cells are identical, so $f_{ijk}(\boldsymbol{q}) = f_0(\boldsymbol{q})$. The amplitude becomes:

$$A^*_{\mathrm{m}}(\boldsymbol{q}) = f_0(\boldsymbol{q}) \sum_{ijk}^{(\mathrm{inside})} e^{i\boldsymbol{q}\cdot\boldsymbol{r}_{ijk}} \tag{35}$$

To compute the scattering intensity from such a grid-based structure using the Debye equation, the cell form factors must be orientation-independent, i.e., $f_0(\boldsymbol{q}) = f_0(q)$. Orientational independence can be enforced by representing each cell as a Gaussian sphere, as applied in Lytje and Pedersen (2025) for grid-based excluded-volume modeling; see Sec. VI.B.2.

3. Evaluating the orientational average

For large or geometrically complex structures, evaluating the orientational average analytically—for instance, via the Debye equation or a spherical-harmonic expansion (App. A2)—can become computationally expensive. A common alternative is to compute the average numerically by sampling orientations directly. The orientational average takes the generic form:

$$\langle f(\boldsymbol{q}\cdot\boldsymbol{r})\rangle_\Omega = \frac{1}{4\pi}\int_{S^2} f(\boldsymbol{q}\cdot\boldsymbol{r})d\Omega \tag{36}$$

where the factor $1\,/\,4\pi$ normalizes the integral over the unit sphere.

As noted in Sec. II.D.5, this average can be carried out in two equivalent ways: rotating the molecule with $\boldsymbol{q}$ fixed, $\langle\cdot\rangle_{\Omega_r}$, or rotating $\boldsymbol{q}$ with the molecule fixed, $\langle\cdot\rangle_{\Omega_q}$. The latter is what enables the numerical method below: rather than reorienting a possibly complex molecular structure, one samples $\boldsymbol{q}$-vectors uniformly on spheres in q-space.

Using the Monte Carlo estimator introduced above, the angular integral in Eq. 36 is approximated by sampling N vectors $\boldsymbol{q}_i$ uniformly on the sphere of radius q, evaluating the scattering for each, and averaging. This approach is widely used in structural validation and refinement workflows (Bardhan *et al.*, 2009; Ginsburg *et al.*, 2019; Knight and Hub, 2015; Poitevin *et al.*, 2011). Uniform sampling of the sphere (not θ and ϕ) is essential for accuracy; see (Blech *et al.*, 2024) for efficient strategies.

VI. MODELING WITH ATOMISTIC STRUCTURES

Having explored modeling strategies for cases with limited prior information, we now turn to situations where an atomistic structural model is available—typically from crystallography, NMR, or cryo-EM—and ask the central validation question of structural biology: does the model reproduce the observed scattering?

Two broad traditions address this question. The conventional approach, exemplified by tools such as *CRYSOL* (Svergun *et al.*, 1995), decomposes the scattering into separately modeled molecular, hydration-shell, and excluded-volume components. The MD-based approach, following Park *et al.* (2009), simulates molecule and solvent together and computes the scattering directly from the trajectory. These two traditions have largely developed in parallel and are rarely connected in the literature. In the following, we examine each through the lens of the framework developed previously.

A. Clarifying the role of the modeling volume

In Sec. III.B, the molecular volume V_{m} is defined to extend beyond the physical molecule and its structured

solvent layer, with its boundary lying in bulk solvent. To compute the intensity $\Delta I^*_{\mathrm{m}}(q)$ emerging from V_{m}, intensity contributions from everything inside—the molecule, solvent, and their coupling—needs to be modeled. Hence, we refer to it also as the *modeling* volume in the following.

After direct background subtraction (Eq. 27), the measured intensity takes the form:

$$I_{\mathrm{A}}^{(\mathrm{exp})}(q) - I_{\mathrm{B}}^{(\mathrm{exp})}(q) = N\big[\Delta I^*_{\mathrm{m}}(q) - \Delta I_{\mathrm{b}}^{(V_{\mathrm{m}})}(q)\big] \quad (37)$$

Two quantities must therefore be modeled: the excess molecular scattering $\Delta I^*_{\mathrm{m}}(q)$ from the structure within V_{m}, and the excess buffer scattering $\Delta I_{\mathrm{b}}^{(V_{\mathrm{m}})}(q)$ from an equivalent volume of pure buffer. The remainder of this section addresses each in turn.

B. Modeling the excess molecular scattering

Within the modeling volume, the excess density can be decomposed into contributions from two physical components: the molecular interior and the hydration shell, relative to a uniform excluded-volume term:

$$\Delta\rho^*_{\mathrm{m}}(\boldsymbol{r},t) = \begin{Bmatrix} \rho'_{\mathrm{m}}(\boldsymbol{r},t) & \text{if } \boldsymbol{r}\in V'_{\mathrm{m}} \\ \rho_{\mathrm{hs}}(\boldsymbol{r},t) & \text{if } \boldsymbol{r}\in V_{\mathrm{hs}} \end{Bmatrix} - \rho_{\mathrm{exv}} \quad (38)$$

where V'_{m} denotes the volume of the bare molecule; V_{hs} the volume of the solvent region including the hydration shell and any additional bulk solvent. Together, V'_{m} and V_{hs} covers the whole modeling volume. The term $\rho_{\mathrm{exv}} \equiv \rho_{\mathrm{b}}$ is the excluded-volume contribution, for which we use a new symbol for consistency with the literature.

This leads to the expansion:

$$\begin{aligned}\Delta I^*_{\mathrm{m}}(q) &= \langle|\Delta A^*_{\mathrm{m}}(\boldsymbol{q},t)|^2\rangle_N \\ &= \langle|A'_{\mathrm{m}}(\boldsymbol{q},t) - A_{\mathrm{exv}}(\boldsymbol{q}) + A_{\mathrm{hs}}(\boldsymbol{q},t)|^2\rangle_N \\ &= I'_{\mathrm{m}}(q) + I_{\mathrm{exv}}(q) + I_{\mathrm{hs}}(q) + \langle(\text{cross-terms})\rangle_N\end{aligned} \quad (39)$$

where $I'_{\mathrm{m}}(q)$ is the scattering of the bare molecule in vacuum, $I_{\mathrm{exv}}(q)$ the contribution from the average buffer density, and $I_{\mathrm{hs}}(q)$ the contribution from the solvent surrounding the molecule. These constitute the three main components that must be modeled, together with their mutual cross-terms.

1. Molecular scattering in vacuum

With an atomistic reference structure available, evaluating the molecular scattering $I'_{\mathrm{m}}(q)$ is a straightforward application of the Debye equation or spherical harmonic expansion (App. A2). We will therefore not discuss this contribution further here; for practical implementations, see (Ginsburg *et al.*, 2019; Grudinin *et al.*, 2017; Gumerov *et al.*, 2012; Lytje and Pedersen, 2025).

2. Excluded volume scattering

The excluded volume scattering amplitude is given as:

$$A_{\mathrm{exv}}(\boldsymbol{q}) = \int_{V_{\mathrm{m}}} \rho_{\mathrm{exv}}\, e^{i\boldsymbol{q}\cdot\boldsymbol{r}} d\boldsymbol{r} \quad (40)$$

The challenge lies in determining the most efficient and accurate approach for evaluating this integral.

Choosing V_{m} to be a simple geometric shape—a sphere or ellipsoid, for instance—makes the integral one of the analytical shape models from Sec. V.B. This is computationally convenient, but the resulting modeling volumes are typically large, and may be prohibitively expensive to fill with solvent in the next step.

To avoid this issue, one can instead discretize V_{m} using e.g. the grid decomposition described in Sec. V.C.2, thus partitioning the integral into small, easily evaluated subunits. To avoid the orientation-dependent issues arising from using cubic form factors, Gaussian spheres may be used to approximate the uniform density (Lytje and Pedersen, 2025).

A common simplification in conventional models is to split the excluded-volume integral into two regions: the physical molecular volume V'_{m} and the surrounding hydration-shell region V_{hs}. The excluded-volume contribution within V_{hs} is then absorbed into the hydration density via an excess form $\Delta\rho_{\mathrm{hs}} \equiv \rho_{\mathrm{hs}} - \rho_{\mathrm{exv}}$, leaving only V'_{m} to be modeled explicitly. This enables the use of excluded-volume models based on the atomic positions of the molecule, including grid-decomposition strategies either with (Lytje and Pedersen, 2025) or without (Bardhan *et al.*, 2009) unit-cell form factors.

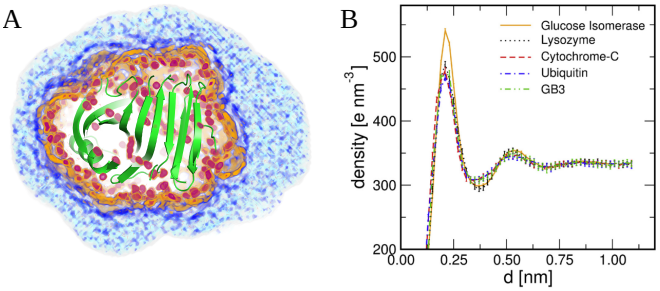
An additional simplification approximates V'_{m} as a sum of atomic contributions, reducing the excluded-volume integral to a discrete sum over the molecule's atoms:

$$A_{\mathrm{exv}}(\boldsymbol{q}) = \int_{V_{\mathrm{m}}} \rho_{\mathrm{exv}}\, e^{i\boldsymbol{q}\cdot\boldsymbol{r}} d\boldsymbol{r} \approx \sum_{i=1}^{N} f_i^{\mathrm{x}}(\boldsymbol{q}) e^{i\boldsymbol{q}\cdot\boldsymbol{r}_i}$$

where $f_i^{\mathrm{x}}(\boldsymbol{q})$ are excluded-volume form factors dependent on atomic size, commonly modeled as Gaussian spheres following the Fraser model (Fraser *et al.*, 1978; Lytje and Pedersen, 2025; Svergun *et al.*, 1995). Sharing atomic positions with the molecular contribution lets the two be combined into a single effective form factor:

$$A'_{\mathrm{m}}(\boldsymbol{q}) - A_{\mathrm{exv}}(\boldsymbol{q}) \approx \sum_{i=1}^{N} f_i^{\mathrm{red}}(\boldsymbol{q}) e^{i\boldsymbol{q}\cdot\boldsymbol{r}_i}, \quad (41)$$

FIG. 17 Solvent density shell from MD simulations. (A) Molecule (green) surrounded by solvent, color-coded by density. (B) Radial solvent density profile showing two density peaks; the second shell is faintly visible in (A). Adapted with permission from Linse and Hub (2023) and Chen and Hub (2014).



where $f_i^{\mathrm{red}}(\boldsymbol{q}) = f_i(\boldsymbol{q}) - f_i^{\mathrm{x}}(\boldsymbol{q})$ is the *reduced form factor* of atom i.

This approximation introduces two systematic errors. First, replacing the continuous density ρ_{exv} with Gaussian densities at atomic positions introduces artificial internal structure into the excluded-volume term, contributing deviations at wide angles. Second, the subtracted density depends on the chosen atomic volume table—still typically taken from Traube (1895)—and on local atomic packing, producing spurious variation across the molecule; for chemically heterogeneous systems such as protein/RNA or protein/detergent complexes, these variations affect the large-scale density distribution and can bias the model even at small angles. Given these problems and the additional issues identified in recent work (Bardhan *et al.*, 2009; Chatzimagas and Hub, 2022; Lytje and Pedersen, 2025), we recommend against the Fraser approximation in new work.

3. Hydration shell scattering

Formed by polar and hydrogen-bonding interactions with the molecular surface, the hydration shell represents a pronounced perturbation of the local solvent density relative to bulk water (Fig. 17). To achieve a bulk-like density at the boundary of V_{m}, the modeling volume should ideally encompass *all* solvent perturbations around the molecule.

In practice, most models compromise by including only the primary overdense shell (Fig. 17B), and neglecting secondary hydration layers. In the language of Sec. VI.A, this corresponds to an effective modeling volume smaller than V_{m}, truncating solvent dentity variations that would otherwise contribute to the scattering signal.

Modeling approaches fall into two broad categories: *explicit* models, in which solvent molecules are represented individually (e.g. MD-based methods), and *implicit* models, in which the solvent distribution is described analytically using e.g. envelope functions (Svergun *et al.*, 1995) or Poisson–Boltzmann-based techniques (Poitevin *et al.*, 2011). These categories differ in how they handle the truncation: explicit models can capture the full solvent density profile within the modeling volume, while implicit models typically restrict their attention to the primary shell. For comparative reviews of the implementations across software packages, see Trewhella *et al.* (2024) and Lytje and Pedersen (2025).

A separate consideration is that larger cavities inside the molecule may contain solvent that contributes to the signal (Matthews and Liu, 2009) and must be modeled in addition to the surface hydration shell.

4. The conformational average in practice

The discussion so far has treated the conformational average $\langle\cdot\rangle_N$ as a formal operation. In practice, the full equilibrium ensemble is rarely available, and modeling reduces to choosing how to approximate this average from limited data.

Within this framework, the various strategies in the literature—rigid-body refinement, conformer pool generation, MD trajectories, Debye–Waller corrections, and normal-mode analysis—are all approximations of $\langle\cdot\rangle_N$. They differ primarily in the timescales they capture (from fast atomic fluctuations to slow collective motions) and in how they sample conformational space (from single structures to heterogeneous all-atom ensembles). Each adds modeling freedom and potential for overfitting; the appropriate choice depends on data quality, the dominant motions of the system, and on the availability of complementary data (e.g. from NMR spectroscopy) that may help to test proposed structural models against overfitting.

C. Modeling the excess buffer scattering

We now turn to the second term in Eq. 37: $\Delta I_{\mathrm{b}}^{(V_{\mathrm{m}})}(q)$, representing the excess scattering of pure buffer within the modeling volume. As noted in Sec. IV, volume-corrected background subtraction absorbs this term into a volume rescaling, removing the need to evaluate it explicitly. For modeling of wide-angle SAS data, however, the volume-corrected approximation is problematic owing to neglecting the cross-term $\Delta C_{\mathrm{b,b}}^{V_{\mathrm{m}},V_{\mathrm{B}}}(q)$. Hence, for such cases, the direct subtraction scheme is preferable, yet requires computation of $\Delta I_{\mathrm{b}}^{(V_{\mathrm{m}})}(q)$.

Evaluating the buffer intensity analytically is complicated by three interlocking issues: buffer composition (water plus experiment-specific additives), geometry (the integral must be evaluated over V_m, whose shape is determined by the molecule), and the need to describe density fluctuations relative to bulk rather than absolute densities. Taken together, a general closed-form expression becomes impossible.

Progress can be made by reframing the problem in terms of local solvent structure. As shown in App. A3, the total buffer scattering can be decomposed into contributions from locally correlated solvent environments; alternatively, the cross-term can be expressed in terms of the bulk pair-correlation function (App. A1.2). Both routes reduce the problem from evaluating scattering over the full modeling volume to tabulating short-range bulk solvent properties, which are accessible from e.g. MD simulations. The remainder of this section therefore takes MD as a modeling approach, and describes how it fits into the theoretical framework developed above.

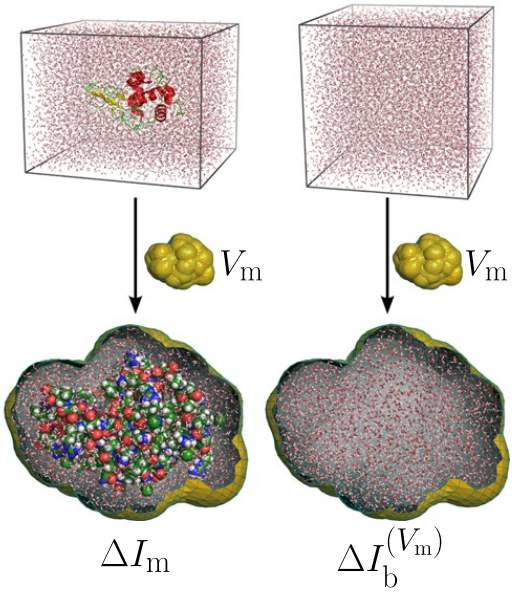
D. The theory behind molecular dynamics simulations

In Sec. VI.C we introduced molecular dynamics (MD) as a practical route to evaluate the pure buffer contribution. MD, however, is not restricted to this isolated task: by explicitly simulating both solute and solvent inside the modeling volume, it provides a direct route to estimating the molecular term and, ultimately, the full observable scattering signal.

Unlike the separate excluded-volume, hydration-shell, and conformational-ensemble treatments discussed earlier, MD captures all these effects naturally through the explicit time evolution of the entire modeling volume. At the same time, MD predictions depend on the forcefield, water model, and sampling length, and remain computationally demanding (Linse and Hub, 2023). MD is therefore a complementary tool, best suited for high-resolution or wide-angle data where detailed solvation and conformational sampling are essential.

Although the discussion below is framed in terms of `WAXSiS` (Knight and Hub, 2015), the underlying principles apply to any explicit-solvent scattering calculation based on MD trajectories. This section focuses on how MD-based calculations connect to the theoretical framework established above, rather than on the practical details of running MD simulations for SAS. For the latter, see Chatzimagas and Hub (2022).

FIG. 18 Two-box setup for accurate MD-based scattering calculations. System A (molecule + solvent) and System B (solvent only) together enable exact modeling of the experimental scattering signal. Adapted from Knight and Hub (2015).



1. Modeling the observed scattering with MD

To model both intensities in Eq. 37, two simulation boxes are required:

System A: The molecule in explicit solvent, within a large simulation box. The scattering calculation is later restricted to the modeling volume V_m.

System B: An otherwise identical simulation box containing only solvent molecules.

From System A we compute the excess molecular intensity:

$$\Delta I_\mathrm{A}^{(\mathrm{MD})}(q) \equiv \langle \Delta I_\mathrm{m}^*(\boldsymbol{q},t)\rangle_N$$

which is in principle sufficient for comparison with volume-corrected experimental profiles. To match the more accurate direct subtraction scheme, however, we also need the corresponding pure-buffer term:

$$\Delta I_\mathrm{B}^{(\mathrm{MD})}(q) \equiv \langle \Delta I_\mathrm{b}^{(V_\mathrm{m})}(\boldsymbol{q},t)\rangle_N$$

representing the scattering from a buffer-only realization of the same modeling volume.

Subtracting the two simulated contributions yields:

$$I_\mathrm{A}^{(\mathrm{exp})}(q) - I_\mathrm{B}^{(\mathrm{exp})}(q) = N\big[\Delta I_\mathrm{A}^{(\mathrm{MD})}(q) - \Delta I_\mathrm{B}^{(\mathrm{MD})}(q)\big] \tag{42}$$

showing that MD naturally implements the exact direct subtraction scheme.

2. Interpretation and equivalence to analytical theory

Although Eq. 42 resembles an experimental background subtraction, the MD calculation reconstructs the two excess terms required by Eq. 37 and crucially does not repeat the experiment.

As shown in App. A4, this formulation is equivalent to that of Park *et al.* (2009): MD-based scattering is therefore not a separate theoretical framework but an explicit-solvent realization of the familiar atomic + hydration-shell + excluded-volume decomposition that underlies conventional analytical methods. The accuracy of both is governed by the same assumptions—choice of modeling volume, treatment of excess solvent density, boundary cross-terms—made implicit in the simulation setup rather than explicit in the model. The conventional and MD-based traditions, long developed in parallel, are thus two realizations of the framework developed here.

VII. DISCUSSION AND CONCLUSIONS

Although small-angle solution scattering is based on simple wave interference, the theory of SAS has often been presented as a collection of largely separate topics, such as diffraction physics, buffer subtraction, analytical models for idealized shapes, or SAS curve predictions based on either implicit or explicit solvent models. In this work, we instead develop a unified theory of small-angle scattering of generic solutes such as biomolecules or soft-matter complexes. We emphasize that these seemingly distinct concepts are aspects of a single framework, and that different analysis and modeling strategies emerge from it through distinct assumptions and approximations. By deriving the framework from first principles and by stating all assumptions and approximations explicitly, we aim to make the theory of SAS accessible to experimentalists, modelers, newcomers, and experienced practitioners alike.

Making the approximations explicit clarifies several points that are often left implicit in introductions to SAS. First, the concept of excess density should not be conflated with buffer subtraction. The sensitivity of SAS signals to excess density follows from Babinet's principle and is intrinsic to the scattering process. Buffer subtraction serves to isolate the scattering signal from the molecule from that of the large contribution arising from the internal structure of bulk water. As emphasized here, buffer subtraction is also an integral part of the theoretical model.

Consequently, the modeling strategy must be compatible with the applied buffer-subtraction scheme to avoid systematic errors. Direct and volume-corrected buffer subtraction are not interchangeable, as they lead to markedly different SAS curves at wide angles, where water scattering dominates, and even to significant variations at intermediate scattering angles. The two schemes furthermore differ in their treatment of the cross-term at the molecule–solvent boundary. In direct subtraction, the cross term cancels exactly against the corresponding contribution from a pure-buffer reference of equivalent volume. In contrast, in volume-corrected subtraction, contributions from the cross-term remain but are typically neglected, rendering this approach approximate when analyzed with standard modeling software. This approximation is most relevant at wider angles, where water–water correlations across the boundary contribute. The two subtraction schemes also differ in that only direct subtraction requires calculating the residual bulk-solvent term—a quantity MD simulations are well suited to provide—and avoiding this calculation is part of what makes the volume-corrected scheme attractive. Thus, the two schemes require different modeling strategies, and reliable analysis of SAS data depends on using compatible combinations of subtraction and modeling; otherwise, systematic errors may arise that are difficult to diagnose.

Within this framework, we derived a range of methods for analyzing SAS curves and for validating structural models against experimental data, including model-free analysis, MD-based approaches, and more conventional structure-based methods. We emphasized that MD-based scattering predictions are not a separate theoretical tradition, but rather an explicit-solvent realization of the same framework, accounting for contributions from the molecule, hydration shell, and excluded volume, as in conventional modeling strategies. By placing these methods within a common framework, this work enables the future comparison and integration of these previously distinct modeling approaches.

Looking forward, this unified framework defines how experimental and modeling choices must be aligned and where their approximations matter. This will become increasingly important as SAS advances toward higher precision, wider scattering angles, time-resolved measurements, and integrative approaches combining scattering with MD simulations. In this regime, distinctions that were negligible at low resolution become quantitatively important. By making assumptions explicit and placing analytical, implicit-solvent, and explicit-solvent methods within a single formal framework, this work provides a foundation for systematically improving SAS methodology and for closer integration between theory, simulation, and experiment.

VIII. ACKNOWLEDGMENTS

K.L. was supported by the Deutsche Forschungsgemeinschaft (DFG, German Research Foundation) via grant HU 1971/3-2 and Danmarks Frie Forskningsfond (DFF, Independent Research Fund Denmark), grant 1026-00209B.

J.S.H. was supported by the DFG, grant INST 256/539-1.

J.S.P. was supported by the Danish Agency for Higher Education and Science (ESS Lighthouse: Colloids and Interfaces in Food and Pharma; Grant No. 726510) and DFF, grant 1026-00209B.

Appendix A1: Computing scattering via correlation functions

The intensity and structure factors derived in Sec. II.D.3 are frequently evaluated in practice using real-space correlation functions, such as the pair correlation function appearing in Eq. 31. This appendix collects and clarifies the connection between the derivation based on scattering amplitudes and the decoupling approximation (Sec. II.D.3) and correlation-based descriptions. We show how the latter are used in analytical theories and molecular simulations.

1. Interpreting the structure factor in terms of correlation functions

In Sec. II.D.3, we expressed the intensity of a correlated molecular system under the decoupling approximation as:[10]

$$I_{\mathrm{s}}(q) = N I^{*}_{\mathrm{m}}(q) S(q) \tag{A1}$$

where the structure factor involves a double-sum over atoms:

$$S(q) = 1 + \frac{\beta(q)}{N} \sum_{i}^{N} \sum_{j\neq i}^{N} \langle e^{i\boldsymbol{q}\cdot\boldsymbol{r}_{ij}} \rangle_{\Omega} \tag{A2}$$

While this form follows naturally from the derivation, it is not directly useful: evaluating the double-sum over molecular positions requires detailed knowledge of exactly how they are distributed. Hence, following Zernike and Prins (1927), we replace the positional sum by a statistical description of the molecular arrangement.

For a fixed reference molecule i, define the local number density of surrounding molecules at displacement $\boldsymbol{r}$ from i:

$$n_i(\boldsymbol{r}) = \sum_{j\neq i}^{N} \delta(\boldsymbol{r} - \boldsymbol{r}_{ij})$$

This is a microscopic quantity: it is sharply peaked at the instantaneous positions of the other $N-1$ molecules. By the sifting property of the delta function, the inner sum over j in Eq. A2 is rewritten as an integral over the density:

$$\sum_{j\neq i}^{N} e^{i\boldsymbol{q}\cdot\boldsymbol{r}_{ij}} = \int_{V_{\mathrm{S}}} n_i(\boldsymbol{r}) e^{i\boldsymbol{q}\cdot\boldsymbol{r}} d\boldsymbol{r},$$

where a discrete sum has been re-expressed as a continuous integral against a sum of delta functions. Orientationally averaging both sides:

$$\sum_{j\neq i}^{N} \langle e^{i\boldsymbol{q}\cdot\boldsymbol{r}_{ij}} \rangle_{\Omega} = \int_{V_{\mathrm{S}}} \langle n_i(\boldsymbol{r}) e^{i\boldsymbol{q}\cdot\boldsymbol{r}} \rangle_{\Omega}\, d\boldsymbol{r}$$

The product average on the right-hand side cannot be evaluated directly. To continue, we adopt a statistical description and replace the microscopic density $n_i(\boldsymbol{r})$ by its ensemble average, $\langle n_i(\boldsymbol{r}) \rangle_N \equiv n_i(r)$ and note that the latter—being spherically symmetric due to the isotropy of the fluid—is independent of the orientation of $\boldsymbol{r}$:

$$\sum_{j\neq i}^{N} \langle e^{i\boldsymbol{q}\cdot\boldsymbol{r}_{ij}} \rangle_{\Omega} = \int_{V_{\mathrm{S}}} n_i(r) \langle e^{i\boldsymbol{q}\cdot\boldsymbol{r}} \rangle_{\Omega}\, d\boldsymbol{r}$$

Although $n_i(\boldsymbol{r})$ is highly anisotropic for any single configuration, its ensemble average $n_i(r)$ is rotationally invariant by the isotropy of the bulk fluid; this is what enables the reduction to radial correlation functions.

Because all reference molecules are statistically equivalent in the bulk, $n_i(r)$ is identical for all molecules, allowing us to drop the index i.

$$n(r) \equiv n g(r)$$

where $n = N/V_{\mathrm{S}}$ is the bulk number density and $g(r)$ is the *radial distribution function*. By construction, $ng(r)dV$ gives the mean number of molecules found in a volume element dV at distance r from a reference molecule. At large separations, where positional correlations vanish, the local density must approach the bulk:

[10] The liquid-state literature commonly starts with the general equation $I_{\mathrm{s}}(q) = \iint_{V_{\mathrm{S}}} \rho(\boldsymbol{r}_1)\rho(\boldsymbol{r}_2)\langle e^{i\boldsymbol{q}\cdot(\boldsymbol{r}_1-\boldsymbol{r}_2)}\rangle_{\Omega}\, d\boldsymbol{r}_1\, d\boldsymbol{r}_2$. While exact, this expression conflates intramolecular and intermolecular contributions within a single integrand: the density $\rho(\boldsymbol{r})$ simultaneously encodes the internal structure of each molecule and the spatial arrangement of molecules relative to one another. Disentangling these two contributions leads to our starting point.

$g(r) \to 1$ as $r \to \infty$. The outer sum over i then contributes a factor of N, since the integrand is now i-independent:

$$\sum_i^N \sum_{j\neq i}^N \langle e^{i\boldsymbol{q}\cdot\boldsymbol{r}_{ij}}\rangle_\Omega = N \int_{V_\mathrm{S}} n g(r) \langle e^{i\boldsymbol{q}\cdot\boldsymbol{r}}\rangle_\Omega \, d\boldsymbol{r} \tag{A3}$$

The structural information accessible to scattering is therefore fully encoded in $g(r)$, with all dependencies on individual molecular positions absorbed into this single radial function.

Eq. A3 is exact under the assumed isotropy and homogeneity, but practically inconvenient: $g(r)$ approaches unity at large r, so the integral receives contributions from the entire integrated volume. To isolate the non-trivial part, we add and subtract unity:

$$\begin{aligned}\sum_i^N \sum_{j\neq i}^N &\langle e^{i\boldsymbol{q}\cdot\boldsymbol{r}_{ij}}\rangle_\Omega \\ &= Nn \int_{V_\mathrm{S}} [g(r) - 1 + 1] \langle e^{i\boldsymbol{q}\cdot\boldsymbol{r}}\rangle_\Omega \, d\boldsymbol{r} \\ &= Nn \int_{V_\mathrm{S}} [g(r) - 1] \langle e^{i\boldsymbol{q}\cdot\boldsymbol{r}}\rangle_\Omega \, d\boldsymbol{r} + Nn \langle \mathcal{S}_{V_\mathrm{S}}(\boldsymbol{q})\rangle_\Omega\end{aligned} \tag{A4}$$

where the shape factor:

$$\langle \mathcal{S}_{V_\mathrm{S}}(\boldsymbol{q})\rangle_\Omega = \int_{V_\mathrm{S}} \langle e^{i\boldsymbol{q}\cdot\boldsymbol{r}}\rangle_\Omega \, d\boldsymbol{r}$$

is identical in form to the one introduced in Eq. 11. Since this contributes only at $q \to 0$ for macroscopic system volumes, it is typically dropped. When the integration domain is small, however, such as when modeling correlations within the molecular volume V_m, the shape factor may contribute significantly and must be retained.

Inserting Eq. A4 into the structure factor of Eq. A2, and dropping the shape factor for macroscopic volumes:

$$S(q) - 1 = n\,\beta(q) \int_{V_\mathrm{S}} [g(r) - 1] \langle e^{i\boldsymbol{q}\cdot\boldsymbol{r}}\rangle_\Omega \, d\boldsymbol{r} \tag{A5}$$

As the integrand decays on distances of order bulk correlation length, the integrated volume may be truncated to a small region around the reference molecule for practical evaluations. Taking the orientational average with Eq. 9, the familiar textbook identity:

$$S(q) - 1 = 4\pi n \int_0^\infty r^2 [g(r) - 1] \operatorname{sinc} qr \, dr$$

is recovered in the limit $\beta(q) \to 1$, which holds exactly for spherically symmetric scatterers and is implicitly assumed in liquid-state treatments where particles are taken as point scatterers from the outset. For anisotropic molecules at finite q, $\beta(q)$ introduces a form-factor-dependent attenuation of the apparent structure factor—a known source of systematic error when fitting $S(q)$ to scattering data from non-spherical particles (Kotlarchyk and Chen, 1983).

a. The excess decoupling ratio $\Delta\beta(q)$

Eq. 24 shows that, for small-angle solution scattering, the relevant quantity is the *excess* density distribution. The preceding section, however, followed the spirit of Sec. II and worked throughout with *absolute* densities. Since $S(q)$ depends on the density through $\beta(q)$, we here examine if introducing $\Delta\beta(q)$ is required to maintain consistency.

Replacing A^*_m with ΔA^*_m in the definition of $\beta(q)$ yields the excess analog:

$$\Delta\beta(q) \equiv \frac{|\langle \Delta A^*_\mathrm{m}(\boldsymbol{q})\rangle_\Omega|^2}{\langle |\Delta A^*_\mathrm{m}(\boldsymbol{q})|^2\rangle_\Omega} = \frac{|\langle A^*_\mathrm{m}(\boldsymbol{q})\rangle_\Omega - \rho_\mathrm{b}\langle \mathcal{S}_{V_\mathrm{m}}(\boldsymbol{q})\rangle_\Omega|^2}{\langle |A^*_\mathrm{m}(\boldsymbol{q}) - \rho_\mathrm{b}\mathcal{S}_{V_\mathrm{m}}(\boldsymbol{q})|^2\rangle_\Omega} \tag{A6}$$

Although $\Delta\beta(q)$ and $\beta(q)$ are constructed from different amplitudes, they coincide exactly in two limits. For homogeneous $\rho^*_\mathrm{m}(\boldsymbol{r})$, the two reduce to the same expression — a non-trivial cancellation, since subtracting a non-zero quantity in both numerator and denominator does not generally leave the ratio invariant.[11] For spherically symmetric V_m, the shape integral is orientation-independent, and $\beta(q) = \Delta\beta(q) = 1$ identically, regardless of the internal density. Typical biomolecules are close to those limiting cases—globular shapes are nearly spherical, and the excess density varies modestly on the typical length scales probed by SAS—so $\Delta\beta(q) \approx \beta(q)$ is a good approximation across the relevant q-range. We use $\Delta\beta(q)$ in subsequent derivations where it arises naturally, but note that it may be replaced by $\beta(q)$ when convenient.

2. Practically using correlation functions to estimate the cross-term

In Sec. III.C.4, the cross-term $\Delta C^{V_\mathrm{m},V_\mathrm{B}}_{\mathrm{b,b}}(q)$ was argued to be nonzero but to cancel upon direct background subtraction. Here, we derive an explicit expression for it in terms of the bulk solvent pair-correlation function, confirming that it is indeed nonzero, and showing explicitly how it may be estimated from bulk-solvent MD simulations.

---

[11] Explicitly, $A^*_\mathrm{m}(\boldsymbol{q}) = \rho^*_\mathrm{m}\mathcal{S}_{V_\mathrm{m}}(\boldsymbol{q})$ and $\Delta A^*_\mathrm{m}(\boldsymbol{q}) = (\rho^*_\mathrm{m} - \rho_\mathrm{b})\mathcal{S}_{V_\mathrm{m}}(\boldsymbol{q})$, so $\Delta\beta(q) = |\langle \mathcal{S}_{V_\mathrm{m}}(\boldsymbol{q})\rangle_\Omega|^2 / \langle |\mathcal{S}_{V_\mathrm{m}}(\boldsymbol{q})|^2\rangle_\Omega = \beta(q)$.

We begin from the single-molecule cross-term:

$$\Delta C_{\mathrm{b,b}}^{V_\mathrm{m},V_\mathrm{B}}(q) = \langle \Delta A_\mathrm{b}^{(V_\mathrm{m})}(\boldsymbol{q},t)\overline{\Delta A_\mathrm{b}^{(V_\mathrm{B})}(\boldsymbol{q},t)}\rangle_N + \mathrm{c.c.}$$

As in Sec. II.D.2, we express each amplitude as a discrete sum over the individual solvent molecules in each region:

$$\Delta A_\mathrm{b}^{(V_\alpha)}(\boldsymbol{q},t) = \sum_{i\in V_\alpha} \Delta A_\mathrm{bm}(\boldsymbol{q},\omega_i) e^{i\boldsymbol{q}\cdot\boldsymbol{r}_i} \qquad \alpha \in \{\mathrm{m},\mathrm{B}\}$$

where $A_\mathrm{bm}(\boldsymbol{q},\omega_i)$ is the amplitude of a single bulk molecule ("bm") in orientation ω_i. Approximating all solvent molecules by the representative structure:

$$\Delta C_{\mathrm{b,b}}^{V_\mathrm{m},V_\mathrm{B}}(q) = \sum_{i\in V_\mathrm{m}}\sum_{j\in V_\mathrm{B}} \langle \Delta A_\mathrm{bm}^*(\boldsymbol{q},\omega_i)\overline{\Delta A_\mathrm{bm}^*(\boldsymbol{q},\omega_j)} e^{i\boldsymbol{q}\cdot\boldsymbol{r}_{ij}}\rangle_\Omega + \mathrm{c.c.}$$

Applying the decoupling approximation, the orientational and positional averages factorize as in Sec. II.D.3:

$$\Delta C_{\mathrm{b,b}}^{V_\mathrm{m},V_\mathrm{B}}(q) = 2|\langle \Delta A_\mathrm{bm}^*(\boldsymbol{q})\rangle_\Omega|^2 \sum_{i\in V_\mathrm{m}}\sum_{j\in V_\mathrm{B}} \langle e^{i\boldsymbol{q}\cdot\boldsymbol{r}_{ij}}\rangle_\Omega$$

where the complex conjugate term has been absorbed into the factor of 2. Recognizing that $|\langle \Delta A_\mathrm{bm}^*(\boldsymbol{q})\rangle_\Omega|^2 = \Delta I_\mathrm{bm}^*(q)\Delta\beta(q)$:

$$\Delta C_{\mathrm{b,b}}^{V_\mathrm{m},V_\mathrm{B}}(q) = 2\Delta I_\mathrm{bm}^*(q)\Delta\beta(q) \sum_{i\in V_\mathrm{m}}\sum_{j\in V_\mathrm{B}} \langle e^{i\boldsymbol{q}\cdot\boldsymbol{r}_{ij}}\rangle_\Omega \quad \text{(A7)}$$

To proceed, we rewrite the positional double sum as an integral over the bulk-solvent radial distribution function, noting that correlations depend only on intermolecular separation:

$$\begin{aligned}
&\sum_{i\in V_\mathrm{m}}\sum_{j\in V_\mathrm{B}} \langle e^{i\boldsymbol{q}\cdot\boldsymbol{r}_{ij}}\rangle_\Omega \\
&\quad = \sum_{i\in V_\mathrm{m}} n_\mathrm{b}\int_{V_\mathrm{B}} g_\mathrm{b}(|\boldsymbol{r}-\boldsymbol{r}_i|)\langle e^{i\boldsymbol{q}\cdot(\boldsymbol{r}-\boldsymbol{r}_i)}\rangle_\Omega \, d\boldsymbol{r} \\
&\quad = n_\mathrm{b}^2 \int_{V_\mathrm{m}}\int_{V_\mathrm{B}} g_\mathrm{b}(|\boldsymbol{r}_1-\boldsymbol{r}_2|)\,\mathrm{sinc}(q|\boldsymbol{r}_1-\boldsymbol{r}_2|)\, d\boldsymbol{r}_1 d\boldsymbol{r}_2
\end{aligned} \quad \text{(A8)}$$

where $n_\mathrm{b} = N_\mathrm{B}/V_\mathrm{B}$ is the bulk number density, $g_\mathrm{b}(r)$ the bulk solvent radial distribution function, and, because isotropy is broken by the boundary, the outer sum was retained as an explicit integral over V_m rather than collapsed into a factor of N as in the homogeneous case. Here, the use of the *bulk*-solvent radial distribution function is justified by the fact that the modeling volume is chosen such that its boundary lies in bulk solvent.

This is the most general form of the cross-correlational term. To practically evaluate it, simplifying assumptions are required.

a. Practically evaluating the cross-term

The cross-term Eq. A8 can be evaluated analytically if V_m is taken as a sphere with radius R, see the Supplementary Information S1 for the full derivation. The result is:

$$\begin{aligned}
\Delta C_{\mathrm{b,b}}^{V_\mathrm{m},V_\mathrm{B}}(q) &= 8\pi^2 n_\mathrm{b}^2 R^2 \Delta\beta(q)\Delta I_\mathrm{bm}^*(q) \\
&\quad \times \int_0^\infty [g_\mathrm{b}(s)-1]\,\mathrm{sinc}(qs) s^3\, ds
\end{aligned} \quad \text{(A9)}$$

where $\Delta I_\mathrm{bm}^*(q)$ is the intensity of a representative bulk water molecule, and we have dropped the boundary terms. The cross-term scales with R^2, i.e. the surface area of the modeling volume, consistent with the surface-area argument of Sec. III.C.4. This scaling reflects the fact that only solvent pairs straddling the boundary contribute. The integral is nonzero since $g_\mathrm{b}(s) \neq 1$ for $s \lesssim \xi$, with ξ being the bulk correlation length, demonstrating that the cross-term does contribute to the observable scattering.

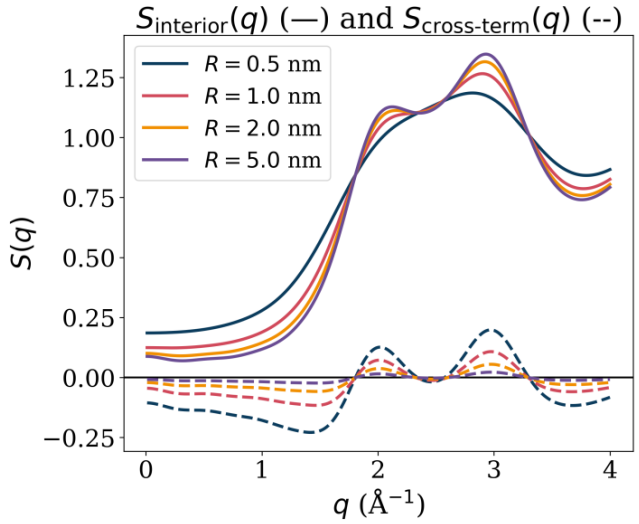
To assess the practical relevance of the cross-term, we compare it to the buffer intensity of the modeling volume itself, $I_\mathrm{b}^{(V_\mathrm{m})}(q) = N_\mathrm{bm}\Delta I_\mathrm{bm}^*(q) S_\mathrm{interior}(q)$, where $N_\mathrm{bm} = n_b V_\mathrm{m}$ is the number of solvent molecules in V_m and $S_\mathrm{interior}(q)$ is the conventional structure factor (Eq. A2) applied to the bulk solvent within V_m. To enable a direct comparison, we recast Eq. A9 in the same form by defining a cross-term structure factor:

$$S_\mathrm{cross}(q) \equiv \frac{8\pi^2 n_\mathrm{b}^2 R^2 \Delta\beta(q)}{N_\mathrm{bm}} \int_0^\infty [g_\mathrm{b}(s)-1]\,\mathrm{sinc}(qs) s^3\, ds, \quad \text{(A10)}$$

so that $\Delta C_{\mathrm{b,b}}^{V_\mathrm{m},V_\mathrm{B}}(q) = N_\mathrm{bm}\Delta I_\mathrm{bm}^*(q) S_\mathrm{cross}(q)$. Unlike S_interior, this S_cross contains no self-pair contribution—the cross-region geometry forbids $i = j$ pairs—and consequently lacks the $+1$ baseline of the conventional structure factor.

To evaluate these two contributions, we computed the oxygen-oxygen radial distribution function g_OO from a 1 µs bulk-solvent MD simulation with the TIP4P/2005 water model (Abascal and Vega, 2005). This g_OO was used to evaluate both the interior structure factor (Eq. S8) and the cross-term (Eq. A9) between the interior sphere and a concentric shell of thickness 1.5 nm, beyond which $g_\mathrm{OO}(s)$ has decayed to its bulk value. The result, shown in Fig. A1, confirms that the cross-term is nonzero and oscillatory across the full q-range. The SI quantifies the cross-term's relative magnitude and its $1/R$ scaling for the bulk-only system analyzed here (S1.5); the molecular case requires separate consideration and is discussed there as well.

FIG. A1 The structure factors of the interior (solid) and cross-term (dashed) for spherical modeling volumes of different radii. The interior approaches the bulk-water structure factor as R grows; the cross-term sits on a zero baseline and carries the solvation-peak structure of g_{OO} that the small-R interior has not yet developed. The two structure factors combine additively into an effective total factor, with only the total constrained to be positive, which is why the cross-term can dip below zero.



Appendix A2: Expanding the amplitude into spherical harmonics

In Sec. II.D.5, we derived the Debye equation, which expresses the orientationally averaged scattering intensity of a representative molecular structure. A popular alternative is to expand the scattering amplitude in a series of *spherical harmonics*. These functions form a complete orthogonal basis on the surface of a sphere, dependent only on the angular coordinates (θ, ϕ). The harmonic basis functions are indexed by the degree l (controlling the overall angular variation) and the order m (labeling the dependence on the azimuthal angle)[12]. Fig. A2 illustrates the first few harmonics, showing how angular variation increases with increasing l.

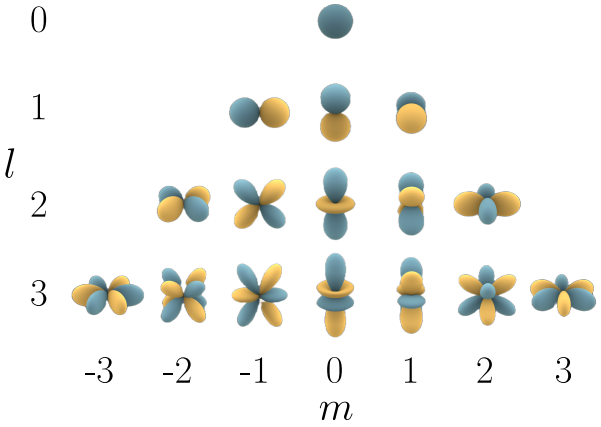
Lord Rayleigh showed that a plane wave may be expanded in terms of spherical harmonic functions as:

$$e^{i\boldsymbol{q}\cdot\boldsymbol{r}} = 4\pi \sum_{l=0}^{\infty} \sum_{m=-l}^{l} i^l j_l(qr) Y_l^m(\hat{\boldsymbol{q}}) \bar{Y}_l^m(\hat{\boldsymbol{r}})$$

where $j_l(qr)$ are spherical Bessel functions and $Y_l^m(\hat{\boldsymbol{r}})$ are spherical harmonics.

[12] As m is an index, it is written in cursive (m), while the "single molecule" label (m) is upright.

FIG. A2 Visualization of the first few spherical harmonic functions. Figure adapted from Quilez (2014).



Substituting this into the definition of the molecular scattering amplitude gives:

$$\begin{aligned} A_{\mathrm{m}}^*(\boldsymbol{q}) &= \int_{V_{\mathrm{m}}} \rho_{\mathrm{m}}^*(\boldsymbol{r}) e^{i\boldsymbol{q}\cdot\boldsymbol{r}} d\boldsymbol{r} \\ &= 4\pi \sum_{l=0}^{\infty} \sum_{m=-l}^{l} i^l Y_l^m(\hat{\boldsymbol{q}}) \int_{V_{\mathrm{m}}} \rho_{\mathrm{m}}^*(\boldsymbol{r}) j_l(qr) \bar{Y}_l^m(\hat{\boldsymbol{r}}) d\boldsymbol{r} \\ &= \sum_{l=0}^{\infty} \sum_{m=-l}^{l} Y_l^m(\hat{\boldsymbol{q}}) A_l^m(q) \end{aligned}$$

where the coefficients are:

$$A_l^m(q) \equiv 4\pi i^l \int_{V_{\mathrm{m}}} \rho_{\mathrm{m}}^*(\boldsymbol{r}) j_l(qr) \bar{Y}_l^m(\hat{\boldsymbol{r}}) d\boldsymbol{r}$$

Squaring and averaging over orientations gives:

$$\begin{aligned} I_{\mathrm{m}}(q) = \langle |A_{\mathrm{m}}^*(\boldsymbol{q})|^2 \rangle_{\Omega_q} &= \frac{1}{4\pi} \int_{\Omega} |A_{\mathrm{m}}^*(\boldsymbol{q})|^2 \, d\Omega_q \\ &= \sum_{l=0}^{\infty} \sum_{m=-l}^{l} |A_l^m(q)|^2 \end{aligned} \tag{A1}$$

where the angular dependence vanishes due to the orthogonality of spherical harmonics. Thus, the intensity is expressed as the squared sum of the expansion coefficients.

1. Practically evaluating the spherical harmonic series

Following Stuhrmann (1970), the coefficients can be computed as a sum over atoms:

$$A_l^m(q) = 4\pi i^l \sum_{j}^{N} f_j(q) j_l(qr_j) \bar{Y}_l^m(\hat{\boldsymbol{r}}_j)$$

The function $A_l^m(q)$ describes how the atomic form factors $f_j(q)$, each modulated by the spherical Bessel function $j_l(qr_j)$, contribute to the overall scattering amplitude. Since $j_l(qr_j)$ is the only term dependent on r_j, it accounts for the radial variation as a function of q.

As the spherical Bessel functions are defined by:

$$j_l(x) \equiv (-x)^l \left(\frac{1}{x}\frac{d}{dx}\right)^l \frac{\sin x}{x}$$

the amplitude acquires a q^l dependence at small q, so only low-order harmonics contribute significantly in this regime. At larger q, higher-order harmonics begin to contribute, allowing finer structural details to be resolved.

To use this method in practice, the series must be truncated at some maximum l, which depends on the desired resolution (Gumerov *et al.*, 2012). The benefit of this widely-used approximation is that Eq. A1 is in principle linear in the number of atoms for fixed l, while the Debye equation is quadratic. This comparison is deceptive, however, as to maintain accuracy, l cannot be kept fixed for higher angles, leading to a similar scaling of the two approaches (Gumerov *et al.*, 2012; Köfinger and Hummer, 2013).

Notably, spherical harmonics are not the only possible basis; they are only used because of their orthogonality on the sphere and natural alignment with angular features. Other bases, such as three-dimensional Zernike polynomials, can also be employed. The choice depends on the geometry and desired convergence properties: spherical harmonics often work well for smoothly varying shapes, whereas Zernike polynomials may offer advantages for structures with internal cavities or complex surfaces (Liu *et al.*, 2012).

Appendix A3: Conformational averaging of the buffer

In Sec. III.C.3, we argued that the buffer may be expressed in terms of locally correlated volumes. Here, we prove this statement. For clarity, the time dependence of volumes and position vectors is suppressed.

The excess instantaneous system intensity is given as:

$$\begin{aligned}\Delta I_{\mathrm{b}}^{(V_{\mathrm{B}})}(\boldsymbol{q},t) &= |\Delta A_{\mathrm{b}}^{(V_{\mathrm{B}})}(\boldsymbol{q},t)|^2 \\ &= \int_{V_{\mathrm{B}}} \Delta\rho_{\mathrm{b}}(\boldsymbol{r}',t)e^{i\boldsymbol{q}\cdot\boldsymbol{r}'}d\boldsymbol{r}' \int_{V_{\mathrm{B}}} \Delta\rho_{\mathrm{b}}(\boldsymbol{r},t)e^{-i\boldsymbol{q}\cdot\boldsymbol{r}}d\boldsymbol{r}\end{aligned}$$

Expressing *only* the outer integral as a sum using Eq. 5:

$$\Delta I_{\mathrm{b}}^{(V_{\mathrm{B}})}(\boldsymbol{q},t) = \sum_i^N e^{i\boldsymbol{q}\cdot\boldsymbol{r}_i}\Delta f_i(\boldsymbol{q}) \int_{V_{\mathrm{B}}} \Delta\rho_{\mathrm{b}}(\boldsymbol{r},t)e^{-i\boldsymbol{q}\cdot\boldsymbol{r}}d\boldsymbol{r}$$

where $\Delta f(\boldsymbol{q})$ now denotes an excess form factor. Assuming short-range solvent correlations, the buffer region around solvent molecule i may be partitioned into its locally correlated environment $V_\xi(i)$ and its uncorrelated complement $V_\xi^{\complement}(i)$:

$$\begin{aligned}\Delta I_{\mathrm{b}}^{(V_{\mathrm{B}})}(\boldsymbol{q},t) &= \sum_i^N \Delta f_i(\boldsymbol{q})\Big\{ \int_{V_\xi(i)} \Delta\rho_{\mathrm{b}}(\boldsymbol{r},t)e^{i\boldsymbol{q}\cdot(\boldsymbol{r}_i-\boldsymbol{r})}d\boldsymbol{r} \\ &\qquad + \int_{V_\xi^{\complement}(i)} \Delta\rho_{\mathrm{b}}(\boldsymbol{r},t)e^{i\boldsymbol{q}\cdot(\boldsymbol{r}_i-\boldsymbol{r})}d\boldsymbol{r}\Big\} \\ &= \sum_i^N \Delta f_i(\boldsymbol{q})\Big\{ \int_{V_\xi(i)} \Delta\rho_{\mathrm{b}}(\boldsymbol{r},t)e^{i\boldsymbol{q}\cdot(\boldsymbol{r}_i-\boldsymbol{r})}d\boldsymbol{r} \\ &\qquad + \sum_j^{\{V_\xi^{\complement}(i)\}} \Delta f_j(\boldsymbol{q})e^{i\boldsymbol{q}\cdot\boldsymbol{r}_{ij}}\Big\}\end{aligned}$$

where the second sum iterates over all molecules in the uncorrelated region. As in the derivation of Eq. 7, the separation vectors $\boldsymbol{r}_{ij}$ in the uncorrelated region are randomly distributed, generating a random walk in the complex plane. For sufficiently large $V_\xi^{\complement}(i)$, the uncorrelated sum vanishes:

$$\begin{aligned}\Delta I_{\mathrm{b}}^{(V_{\mathrm{B}})}(\boldsymbol{q},t) &= \sum_i^N \Delta f_i(\boldsymbol{q})\Big\{ \int_{V_\xi(i)} \Delta\rho_{\mathrm{b}}(\boldsymbol{r})e^{i\boldsymbol{q}\cdot(\boldsymbol{r}_i-\boldsymbol{r})}d\boldsymbol{r}\Big\} \\ &= \sum_i^N \sum_j^{\{V_\xi(i)\}} \Delta f_i(\boldsymbol{q})\Delta f_j(\boldsymbol{q})e^{i\boldsymbol{q}\cdot\boldsymbol{r}_{ij}}\end{aligned}$$

Because the buffer is at equilibrium, all time-evolved conformational states are simultaneously populated, and each solvent molecule samples the same equilibrium distribution of local environments. As in Sec. II.D.2, the outer sum therefore acts as an average over molecules with—on average—identical environments:

$$\begin{aligned}\Delta I_{\mathrm{b}}^{(V_{\mathrm{B}})}(\boldsymbol{q},t) &= \sum_i^N \Delta f_i(\boldsymbol{q}) \sum_j^{\{V_\xi(i)\}} \Delta f_j(\boldsymbol{q})e^{i\boldsymbol{q}\cdot\boldsymbol{r}_{ij}} \\ &\approx N\Big\langle \Delta f^*(\boldsymbol{q}) \sum_j^{\{V_\xi(i)\}} \Delta f_j(\boldsymbol{q})e^{i\boldsymbol{q}\cdot\boldsymbol{r}_{ij}}\Big\rangle_N \\ &= \Delta I_{\mathrm{b}}^{(V_{\mathrm{B}})}(q) \qquad \text{(A1)}\end{aligned}$$

where both the vector-$\boldsymbol{q}$ and time dependence vanish as argued in Sec. III.C.2. For multiple solvent species, the outer sum separates naturally into species-specific terms of the same form.

Intuitively, the buffer may be viewed as a collection of *overlapping* correlation regions centered on each solvent molecule. These locally correlated volumes are the primary contributors to the scattering and are the ones over which the conformational average is performed.

TABLE A2 Overview of how our notation corresponds to that of Park *et al.* (2009).

Notation	Density	Amplitude	Intensity	Averaging
Our work	$\rho(\boldsymbol{r})$	$A(\boldsymbol{q})$	$I(q)$	$\langle\cdot\rangle_N$ (conformations)
Park *et al.*	$A(\boldsymbol{r})$	$\tilde{A}(\boldsymbol{q})$	$I(q)$	$\langle\cdot\rangle_w$ (conformations)

Appendix A4: Equivalence to Park et al.

Several papers concerned with the development of MD-based SAS calculations are based on the seminal paper by Park *et al.* (2009). We show that their main result is equivalent to Eq. 42. For context, their $\tilde{A}_1(\boldsymbol{q})$ and $\tilde{B}_1(\boldsymbol{q})$ refer to the total scattering amplitude of the simulated volume V_m in systems A and B, respectively.

Using our notation (Table A2), their key result is Eq. 26 in their paper:

$$\tilde{I}(q) = N\langle D_{11}(\boldsymbol{q})\rangle_\Omega$$

where:

$$D_{11}(\boldsymbol{q}) = \left|\langle A_\mathrm{m}(\boldsymbol{q},t)\rangle_N - \langle A_\mathrm{b}^{(V_\mathrm{m})}(\boldsymbol{q},t)\rangle_N\right|^2 + \left[\langle|A_\mathrm{m}(\boldsymbol{q},t)|^2\rangle_N - |\langle A_\mathrm{m}(\boldsymbol{q},t)\rangle_N|^2\right] - \left[\langle|A_\mathrm{b}^{(V_\mathrm{m})}(\boldsymbol{q},t)|^2\rangle_N - |\langle A_\mathrm{b}^{(V_\mathrm{m})}(\boldsymbol{q},t)\rangle_N|^2\right] \tag{A1}$$

Here, $A_\mathrm{m}(\boldsymbol{q},t)$ is the amplitude due to the *absolute* molecular density $\rho_\mathrm{m}(\boldsymbol{r},t)$, and $A_\mathrm{b}^{(V_\mathrm{m})}(\boldsymbol{q},t)$ the amplitude due to the *absolute* buffer density, $\rho_\mathrm{b}(\boldsymbol{r},t) = \rho_\mathrm{b} + \Delta\rho_\mathrm{b}(\boldsymbol{r},t)$. To simplify the notation in the following derivations, we define:

$$\begin{aligned} A_\mathrm{b}^{(V_\mathrm{m})}(\boldsymbol{q},t) &= \int_{V_\mathrm{m}} \rho_\mathrm{b} e^{i\boldsymbol{q}\cdot\boldsymbol{r}} d\boldsymbol{r} + \int_{V_\mathrm{m}} \Delta\rho_\mathrm{b}(\boldsymbol{r},t) e^{i\boldsymbol{q}\cdot\boldsymbol{r}} d\boldsymbol{r} \\ &\equiv \Theta(\boldsymbol{q}) + \mathcal{F}(\boldsymbol{q},t) \end{aligned}$$

where the symbols $\Theta(\boldsymbol{q})$ and $\mathcal{F}(\boldsymbol{q},t)$ are used to more clearly indicate later substitutions. Written this way, the amplitude has the two special properties:

i) $\langle A_\mathrm{b}^{(V_\mathrm{m})}(\boldsymbol{q},t)\rangle_N = \Theta(q) + \cancel{\langle\mathcal{F}(\boldsymbol{q},t)\rangle_N}$

since the fluctuations average to zero over all conformations. This implies:

ii) $\langle|A_\mathrm{b}^{(V_\mathrm{m})}(\boldsymbol{q},t)|^2\rangle_N = \langle|\Theta(\boldsymbol{q})|^2\rangle_N + \langle|\mathcal{F}(\boldsymbol{q},t)|^2\rangle_N - \cancel{\langle\Theta(\boldsymbol{q})\rangle_N\overline{\langle\mathcal{F}(\boldsymbol{q},t)\rangle_N}} - \cancel{\langle\mathcal{F}(\boldsymbol{q},t)\rangle_N\overline{\langle\Theta(\boldsymbol{q})\rangle_N}}$

which follows since the average of the product $\langle\mathcal{F}(\boldsymbol{q},t)\Theta(\boldsymbol{q})\rangle_N$ factorizes into the product of averages. The first term in Eq. A1 may be expanded in terms of these as:

$$\begin{aligned} \left|\langle A_\mathrm{m}(\boldsymbol{q},t)\rangle_N - \langle A_\mathrm{b}^{(V_\mathrm{m})}(\boldsymbol{q},t)\rangle_N\right|^2 &= |\langle A_\mathrm{m}(\boldsymbol{q},t)\rangle_N|^2 + |\langle A_\mathrm{b}^{(V_\mathrm{m})}(\boldsymbol{q},t)\rangle_N|^2 - \langle A_\mathrm{m}(\boldsymbol{q},t)\rangle_N\overline{\langle A_\mathrm{b}^{(V_\mathrm{m})}(\boldsymbol{q},t)\rangle_N} - \langle A_\mathrm{b}^{(V_\mathrm{m})}(\boldsymbol{q},t)\rangle_N\overline{\langle A_\mathrm{m}(\boldsymbol{q},t)\rangle_N} \\ &= |\langle A_\mathrm{m}(\boldsymbol{q},t)\rangle_N|^2 + \langle|\Theta(\boldsymbol{q})|^2\rangle_N - \langle A_\mathrm{m}(\boldsymbol{q},t)\rangle_N\overline{\langle\Theta(\boldsymbol{q})\rangle_N} - \langle\Theta(\boldsymbol{q})\rangle_N\overline{\langle A_\mathrm{m}(\boldsymbol{q},t)\rangle_N} \end{aligned}$$

where we have once again used the independence of $\Theta(\boldsymbol{q})$ to distribute the average. Inserting this expansion back into Eq. A1:

$$\begin{aligned} D_{11}(\boldsymbol{q}) &= \left[\cancel{|\langle A_\mathrm{m}(\boldsymbol{q},t)\rangle_N|^2} + \langle|\Theta(\boldsymbol{q})|^2\rangle_N - \langle A_\mathrm{m}(\boldsymbol{q},t)\rangle_N\overline{\langle\Theta(\boldsymbol{q})\rangle_N} - \langle\Theta(\boldsymbol{q})\rangle_N\overline{\langle A_\mathrm{m}(\boldsymbol{q},t)\rangle_N}\right] + \left[\langle|A_\mathrm{m}(\boldsymbol{q},t)|^2\rangle_N - \cancel{|\langle A_\mathrm{m}(\boldsymbol{q},t)\rangle_N|^2}\right] \\ &\quad - \left[\cancel{\langle|\Theta(\boldsymbol{q})|^2\rangle_N} + \langle|\mathcal{F}(\boldsymbol{q},t)|^2\rangle_N - \cancel{\langle|\Theta(\boldsymbol{q})|^2\rangle_N}\right] \\ &= \left[\langle|A_\mathrm{m}(\boldsymbol{q},t)|^2\rangle_N + \langle|\Theta(\boldsymbol{q})|^2\rangle_N - \langle A_\mathrm{m}(\boldsymbol{q},t)\rangle_N\overline{\langle\Theta(\boldsymbol{q})\rangle_N} - \langle\Theta(\boldsymbol{q})\rangle_N\overline{\langle A_\mathrm{m}(\boldsymbol{q},t)\rangle_N}\right] - \langle|\mathcal{F}(\boldsymbol{q},t)|^2\rangle_N \\ &= \langle|A_\mathrm{m}(\boldsymbol{q},t) - \Theta(\boldsymbol{q})|^2\rangle_N - \langle|\mathcal{F}(\boldsymbol{q},t)|^2\rangle_N \\ &= \Delta I_\mathrm{m}(q) - \Delta I_\mathrm{b}^{(V_\mathrm{m})}(q) \\ &= \Delta I_\mathrm{A}^{(\mathrm{MD})}(q) - \Delta I_\mathrm{B}^{(\mathrm{MD})}(q) \end{aligned}$$

Here, we have identified the first term as the excess intensity, as the difference of amplitudes, when integrated over the same volume V_m, can be expressed as a difference of densities. The second term was similarly identified as the excess buffer scattering from system B. This result is equivalent to Eq. 42 followed from our formalism.

Supplementary Information S1: Evaluating the cross-boundary volume integral for spherical domains

In App. A1.2, the cross-term was reduced to the double volume integral:

$$\mathcal{I}(q) \equiv n_b^2 \int_{V_\mathrm{m}} \int_{V_\mathrm{B}} g_\mathrm{b}(|\boldsymbol{r}_1 - \boldsymbol{r}_2|)\,\mathrm{sinc}(q|\boldsymbol{r}_1 - \boldsymbol{r}_2|) d\boldsymbol{r}_2 d\boldsymbol{r}_1$$

We evaluate this integral for a spherical modeling volume V_m of radius R with its concentric complement V_B.

To expose the geometric structure of the integral, we introduce indicator functions $f_\mathrm{m}(\boldsymbol{r}) = \mathbf{1}[\boldsymbol{r} \in V_\mathrm{m}]$ and $f_\mathrm{B}(\boldsymbol{r}) = \mathbf{1}[\boldsymbol{r} \in V_\mathrm{B}]$, which are unity inside their respective domains and zero elsewhere. Multiplying by these functions encodes the domain restrictions as integrand factors rather than integration limits, allowing both integrals to be extended freely to all of V_S:

$$\mathcal{I}(q) = n_b^2 \iint_{V_\mathrm{S}} f_\mathrm{m}(\boldsymbol{r}_1) f_\mathrm{B}(\boldsymbol{r}_2) g_\mathrm{b}(|\boldsymbol{r}_1 - \boldsymbol{r}_2|) \times \mathrm{sinc}(q|\boldsymbol{r}_1 - \boldsymbol{r}_2|) d\boldsymbol{r}_2\, d\boldsymbol{r}_1$$

Substituting $\boldsymbol{s} = \boldsymbol{r}_1 - \boldsymbol{r}_2$:

$$\mathcal{I}(q) = n_b^2 \int_{V_\mathrm{S}} g_\mathrm{b}(s)\,\mathrm{sinc}(qs) \underbrace{\left[\int_{V_\mathrm{S}} f_\mathrm{m}(\boldsymbol{r}_1) f_\mathrm{B}(\boldsymbol{r}_1 - \boldsymbol{s}) d\boldsymbol{r}_1\right]}_{[f_\mathrm{m} \star f_\mathrm{B}](s)} d\boldsymbol{s} \tag{S1}$$

The bracketed inner integral is the cross-correlation of the two indicator functions at separation $\boldsymbol{s}$, counting the total volume of point pairs separated by $\boldsymbol{s}$ with one point in V_m and one in V_B. By the rotational symmetry of the concentric geometry it depends only on $s = |\boldsymbol{s}|$, so the integral reduces to:

$$\mathcal{I}(q) = n_b^2 \int_0^\infty 4\pi s^2 g_\mathrm{b}(s)\,\mathrm{sinc}(qs)[f_\mathrm{m} \star f_\mathrm{B}](s) ds$$

Since $V_\mathrm{B} = V_\mathrm{S} - V_\mathrm{m}$, the indicator functions satisfy $f_\mathrm{B} = 1 - f_\mathrm{m}$, giving the decomposition:

$$[f_\mathrm{m} \star f_\mathrm{B}](s) = \underbrace{[f_\mathrm{m} \star f_\mathrm{S}](s)}_{\mathcal{K}_\mathrm{I}(s)} - \underbrace{[f_\mathrm{m} \star f_\mathrm{m}](s)}_{\mathcal{K}_\mathrm{II}(s)} \tag{S2}$$

The two terms are now evaluated separately.

1. The first term

Since V_S is taken to be all of space, $[f_\mathrm{m} \star f_\mathrm{S}](s)$ counts the volume of all points within V_m for any displacement s, which is simply V_m:

$$\mathcal{K}_\mathrm{I}(s) = V_\mathrm{m}$$

The corresponding contribution to Eq. S1 is:

$$\mathcal{I}_\mathrm{I}(q) = n_b^2 V_\mathrm{m} \int_0^\infty 4\pi s^2 g_\mathrm{b}(s)\,\mathrm{sinc}(qs) ds$$

2. The second term

The second term involves the autocorrelation of the indicator function of V_m:

$$\mathcal{K}_\mathrm{II}(s) = [f_\mathrm{m} \star f_\mathrm{m}](s) = \int f_\mathrm{m}(\boldsymbol{r}) f_\mathrm{m}(\boldsymbol{r} - \boldsymbol{s}) d\boldsymbol{r}$$

This counts the volume of the intersection of V_m with a copy of itself displaced by $\boldsymbol{s}$—the *lens volume* of two identical spheres of radius R whose centres are separated by s.[13] By rotational symmetry it depends only on s and vanishes for $s > 2R$. The result is the standard geometric formula:

$$\Gamma(s) \equiv [f_\mathrm{m} \star f_\mathrm{m}](s) = V_\mathrm{m}\left(1 - \frac{3s}{4R} + \frac{s^3}{16R^3}\right) \qquad s \le 2R \tag{S3}$$

and $\Gamma(s) = 0$ for $s > 2R$. Substituting into Eq. S1:

$$\mathcal{I}_\mathrm{II}(q) = n_b^2 \int_0^\infty 4\pi s^2 g_\mathrm{b}(s)\,\mathrm{sinc}(qs)\Gamma(s) ds$$

3. Combining and isolating the correlation contribution

Taking the difference from Eq. S2:

$$\mathcal{I}(q) = n_b^2 \int_0^\infty 4\pi s^2\, g_\mathrm{b}(s)\ \mathrm{sinc}(qs)\big[V_\mathrm{m} - \Gamma(s)\big]\, ds \tag{S4}$$

Substituting Eq. S3 gives:

$$V_\mathrm{m} - \Gamma(s) = V_\mathrm{m}\left(\frac{3s}{4R} - \frac{s^3}{16R^3}\right) = \pi R^2 s - \frac{\pi}{12} s^3$$

To separate the structural contribution from the purely geometric one, we expand $g_\mathrm{b}(s) = [g_\mathrm{b}(s) - 1] + 1$ as in App. A1:

$$\mathcal{I}(q) = n_b^2 \int_0^\infty 4\pi s^2\,[g_\mathrm{b}(s) - 1]\ \mathrm{sinc}(qs)\big[V_\mathrm{m} - \Gamma(s)\big]\, ds + n_b^2 \int_0^\infty 4\pi s^2\ \mathrm{sinc}(qs)\big[V_\mathrm{m} - \Gamma(s)\big]\, ds \tag{S5}$$

[13] This is commonly referred to as the "ghost image" in the small-angle scattering literature (Feigin and Svergun, 1987; Glatter and Kratky, 1982).

The second integral is a purely geometric boundary term. Since $\Gamma(s)$ is by construction the autocorrelation of f_{m}, and $\mathcal{S}_{V_{\mathrm{m}}}(q) = \int f_{\mathrm{m}}(\boldsymbol{r})\, e^{i\boldsymbol{q}\cdot\boldsymbol{r}} d\boldsymbol{r}$ is its Fourier transform, by the convolution theorem, the Fourier transform of $\Gamma(s)$ is $|\mathcal{S}_{V_{\mathrm{m}}}(q)|^2$. The two parts of the geometric term therefore evaluate to:

$$\begin{aligned} & n_b^2 \int_0^\infty 4\pi s^2 \operatorname{sinc}(qs) \left[V_{\mathrm{m}} - \Gamma(s)\right] ds \\ & \quad = n_b^2 \left[V_{\mathrm{m}} \mathcal{S}_{V_{\mathrm{m}}}(q) - |\mathcal{S}_{V_{\mathrm{m}}}(q)|^2\right] \end{aligned}$$

This term is concentrated near forward scattering for macroscopic volumes and is dropped in what follows.

For the correlation integral in Eq. S5, $g_{\mathrm{b}}(s) - 1$ decays to zero beyond the bulk correlation length $\xi \ll R$, so only $s \lesssim \xi$ contributes. In this regime $V_{\mathrm{m}} - \Gamma(s) \approx \pi R^2 s$,[14] and the cubic correction is negligible:

$$\mathcal{I}(q) \approx n_b^2 \pi R^2 \int_0^\infty 4\pi s^3 [g_{\mathrm{b}}(s) - 1] \operatorname{sinc}(qs) ds \qquad \text{(S6)}$$

Collecting the prefactors from App. A1.2:

$$\begin{aligned} \Delta C_{\mathrm{b,b}}^{V_{\mathrm{m}}, V_{\mathrm{B}}}(q) &= 8\pi^2 n_{\mathrm{b}}^2 R^2 \Delta\beta(q) \Delta I_{\mathrm{bm}}^*(q) \\ &\quad \times \int_0^\infty s^3 [g_{\mathrm{b}}(s) - 1] \operatorname{sinc}(qs) ds \end{aligned} \qquad \text{(S7)}$$

The cross-term scales with R^2, i.e. the surface area of the modeling volume, reflecting the fact that only solvent pairs straddling the boundary of V_{m} contribute to the integral.

4. Comparing with the interior scattering

To assess the relative importance of the cross-term, we compare it with the interior scattering $I_{\mathrm{m}}^*(q) = N I_{\mathrm{bm}}^*(q) S(q)$. Using Eq. A5 with $\Delta\beta(q)$ and dropping the shape-factor term:

$$\begin{aligned} I_{\mathrm{m}}^*(q) &= N \Delta I_{\mathrm{bm}}^*(q) \\ &\quad \times \left\{ 1 + 4\pi n_b \Delta\beta(q) \int_0^\infty s^2 [g_{\mathrm{b}}(s) - 1] \operatorname{sinc}(qs) ds \right\} \end{aligned} \qquad \text{(S8)}$$

Comparing Eq. S8 with Eq. S7, the ratio of the cross-term to the interior scattering is:

$$\begin{aligned} \frac{\Delta C_{\mathrm{b,b}}^{V_{\mathrm{m}}, V_{\mathrm{B}}}(q)}{I_{\mathrm{m}}^*(q)} &= \frac{8\pi^2 n_{\mathrm{b}}^2 R^2 \Delta\beta(q)}{N 1 + 4\pi n_b \Delta\beta(q)} \\ &\quad \times \frac{\displaystyle\int_0^\infty s^3 [g_{\mathrm{b}}(s) - 1] \operatorname{sinc}(qs) ds}{\displaystyle\int_0^\infty s^2 [g_{\mathrm{b}}(s) - 1] \operatorname{sinc}(qs) ds} \end{aligned} \qquad \text{(S9)}$$

[14] This amounts to neglecting curvature terms.

Using $N = 4\pi n_{\mathrm{b}} R^3/3$, the prefactor simplifies to $6\pi n_{\mathrm{b}} \Delta\beta(q)/R$.

The denominator of Eq. S9 interpolates between two physically distinct regimes. At low q, the structure-factor correction is negligible and the denominator is dominated by the form-factor term: $S(q) \approx 1$. In this regime the ratio reduces to:

$$\begin{aligned} \frac{\Delta C_{\mathrm{b,b}}^{V_{\mathrm{m}}, V_{\mathrm{B}}}(q)}{I_{\mathrm{m}}^*(q)} &\xrightarrow{q \to 0} \frac{6\pi n_{\mathrm{b}}}{R} \int_0^\infty s^3 [g_{\mathrm{b}}(s) - 1] ds \\ &\sim \frac{n_{\mathrm{b}} \xi^4}{R} \end{aligned}$$

where $\Delta\beta(q) \to 1$.

$\Delta I_{\mathrm{bm}}^*(q)$ decays rapidly with q as it is the Fourier transform of a smooth single-molecule density. The observed buffer scattering, however, retains structure at wider angles—the nearest-neighbor peaks of liquid water, for example. This structure originates from $g_{\mathrm{b}}(s) - 1$ entering through the structure factor, so at high q the denominator of Eq. S9 is dominated by the correlation integral rather than the form-factor term. Using this approximation:

$$\begin{aligned} \frac{\Delta C_{\mathrm{b,b}}^{V_{\mathrm{m}}, V_{\mathrm{B}}}(q)}{I_{\mathrm{m}}^*(q)} &\longrightarrow \frac{\dfrac{6\pi n_{\mathrm{b}}}{R} \displaystyle\int_0^\infty s^3 [g_{\mathrm{b}}(s) - 1] \operatorname{sinc}(qs) ds}{4\pi n_b \Delta\beta(q) \displaystyle\int_0^\infty s^2 \left[g_{\mathrm{b}}(s) - 1\right] \operatorname{sinc}(qs)\, ds} \\ &\sim \frac{3\xi}{2R} \end{aligned}$$

In both limits the cross-term is suppressed relative to the interior scattering by a factor ξ/R, the ratio of the bulk correlation length to the radius of the modeling volume. For typical aqueous buffers ($\xi \sim$ 3–5 Å) and modeling volumes of radius $R \sim$ 30–100 Å, this amounts to a suppression of one to two orders of magnitude, confirming that the cross-term is a small but nonzero correction that scales with the surface area $4\pi R^2$ of V_{m}.

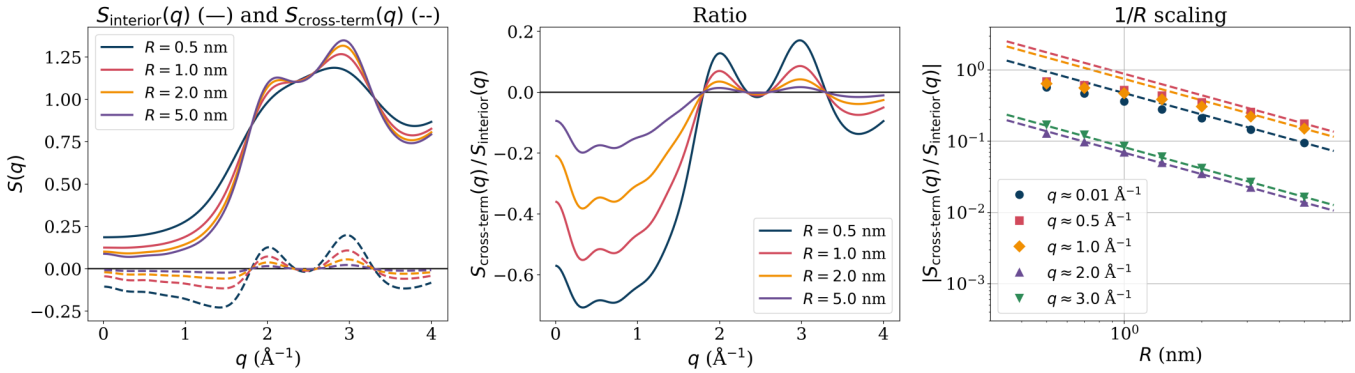
5. Numerical evaluation of the cross-term

The structure factor of the interior Eq. S8 and the cross-term Eq. S7 were evaluated using g_{OO} from a 1 μs bulk-solvent simulation with TIP4P/2005 (Abascal and Vega, 2005), with the cross-term integrated against a concentric shell of 1.5 nm thickness. The results are shown in Fig. S3.

a. Relative importance in the molecular system

The ξ/R scaling derived above is for System B, where V_{m} is filled entirely with bulk solvent. The cross-term

FIG. S3 Numerical evaluation of the cross-term structure factor for spherical V_m. *Left:* Reproduced from Fig. A1 for reference. *Middle:* Ratio $S_{cross}(q)/S_{interior}(q)$, demonstrating that the cross-term is a comparable fraction of the interior structure factor across q. *Right:* Magnitude of the same ratio versus R at fixed q; dashed lines have slope -1, confirming the ξ/R scaling derived above. Deviations at small R correspond to the breakdown of the $\xi \ll R$ approximation.



can be read as a boundary correction: a finite interior does not scatter exactly like bulk water near its surface, and the cross-term restores the missing correlations. As established in Sec. III.C.4, this correction is a purely bulk quantity, fixed by the boundary shell and independent of the molecule at the centre, so it is the same in both systems. It loses importance as R grows only because the bulk-solvent interior it corrects scales as R^3 while the correction scales as R^2. In System A the molecule and its hydration shell occupy the core, leaving only a thin outer shell of bulk-like solvent inside V_m. The boundary correction is unchanged, but the bulk-solvent interior it is weighed against is now far smaller, so the same correction carries much greater relative weight—qualitatively the low-R, or equivalently thin-shell, behaviour of Fig. S3 (right). The all-bulk interior assumed in the figure therefore understates the ratio expected for the molecular system. A quantitative treatment would require a hollow-sphere geometry and lies outside the scope of the present work.

The middle panel must be read with care for the molecular system, as it shows a ratio of structure factors rather than of intensities. In the observable, the cross-term enters weighted by the single-molecule buffer intensity $\Delta I^*_{bm}(q)$, whereas the molecular signal carries its own form factor, which dominates at low q and decays at wider angles. The cross-term is therefore negligible at low q irrespective of the structure-factor ratio, and is most relevant at wider angles where solvent dominates the scattering.

REFERENCES

Abascal, J. L., and C. Vega (2005), Journal of Chemical Physics **123**, 10.1063/1.2121687/965459.

Adams, M., N. Agouzal, G. Alina, Z. Attala, M. Doucet, J. Bakker, P. Beaucage, J. Berger, W. Bouwman, R. Bourne, P. Butler, J. H. Cho, I. Cadwallader-Jones, K. Campbell, T. Cooper-Benun, J. Crake-Merani, G. Drosos, C. Durniak, C. Farrow, R. F. Leal, R. Ford, L. Forster, J. Gaudet, M. Gerina, P. Gilbert, M. Gonzalez, R. Heenan, E. Hewins, A. Jackson, G. Jensen, P. Juhas, S. King, J. Karliczek, P. Kienzle, J. Krzywon, J. Lin, Y. Liu, R. Lopes, D. Lozano, K. Lytje, D. Mannicke, B. Maranville, A. Markvardsen, N. Martinez, M. McKerns, B. Miller, K. Mothander, R. Murphy, A. Nelson, T. Nielsen, L. O'Driscoll, M. Oakley, H. Park, P. Parker, M. Patrou, P. Peterson, W. Potrzebowski, S. Prescott, M. Rakitin, T. Richter, J. Rooks, P. Rozyczko, X. Shan, T. Snow, A. Stellhorn, S. Teixeira, J. Tumarkin, A. Washington, K. Weigandt, R. Whitley, L. Wilkins, C. Wolf, R. C. Hernandez, A. Zhang, and A. Zheng (2024), "Sasview version 6.0.0," .

Als-Nielsen, J., and D. McMorrow (2011), Elements of Modern X-ray Physics: Second Edition 10.1002/9781119998365.

Bardhan, J., S. Park, and L. Makowski (2009), J. Appl. Cryst **42**, 932.

Barker, J. G., and D. F. Mildner (2015), urn:issn:1600-5767 **48**, 1055.

Benoit, H. (1953), Journal of Polymer Science **11**, 507.

Blech, A., R. M. M. Ebeling, M. Heger, C. P. Koch, and D. M. Reich (2024), The Journal of Chemical Physics **161**, 10.1063/5.0230569/3315373.

Born, M. (1926), Zeitschrift für Physik 1926 38:11 **38**, 803.

Caflisch, R. E. (1998), Acta Numerica **7**, 1.

Chatzimagas, L., and J. S. Hub (2022), "Chapter fifteen - predicting solution scattering patterns with explicit-solvent molecular simulations," in *Methods in Enzymology*, Vol. 677, edited by J. A. Tainer (Academic Press) pp. 433–456.

Chen, P. C., and J. S. Hub (2014), Biophysical Journal **107**, 435.

Ciccariello, S., J. M. Schneider, B. Schönfeld, and G. Kostorz (2002), Journal of Applied Crystallography **35**, 304.

Debye, P. (1915), Annalen der Physik **351**, 809.

Debye, P. (1947), Journal of Physical and Colloid Chemistry **51**, 18.

Debye, P., and A. M. Bueche (1949), Journal of Applied Physics **20**, 518.

Deumer, J., B. R. Pauw, S. Marguet, D. Skroblin, O. Taché,

M. Krumrey, and C. Gollwitzer (2022), Journal of applied crystallography **55**, 993.
Feigin, L. A., and D. I. Svergun (1987), Structure Analysis by Small-Angle X-Ray and Neutron Scattering 10.1007/978-1-4757-6624-0.
Fraser, R. D. B., T. P. MacRae, and E. Suzuki (1978), Journal of Applied Crystallography **11**, 693.
Gabel, F., S. Engilberge, E. Schmitt, A. Thureau, Y. Mechulam, J. Pérez, E. Girard, and M. Czjzek (2022), Acta Crystallographica Section D: Structural Biology **78**, 1120.
Ginsburg, A., T. Ben-Nun, R. Asor, A. Shemesh, L. Fink, R. Tekoah, Y. Levartovsky, D. Khaykelson, R. Dharan, A. Fellig, and U. Raviv (2019), Journal of Applied Crystallography **52**.
Glatter, O. (1977), Journal of Applied Crystallography **10**, 415.
Glatter, O., and O. Kratky (1982), *Small Angle X-ray Scattering* (Academic Press).
Griffiths, D. J., and D. F. Schroeter (2018), Introduction to Quantum Mechanics 10.1017/9781316995433.
Grudinin, S., M. Garkavenko, and A. Kazennov (2017), Acta crystallographica. Section D, Structural biology **73**, 449.
Guinier, A. (1939), Annales de la Physique **12**, 161.
Guinier, A., G. Fournet, C. B. Walker, and G. H. Vineyard (1956), Physics Today **9**, 38.
Gumerov, N. A., K. Berlin, D. Fushman, and R. Duraiswami (2012), Journal of Computational Chemistry **33**, 1981.
Hansen, S. (1990), Journal of Applied Crystallography **23**, 344.
Hung, Y. C. (2024), Wiley Interdisciplinary Reviews: Computational Statistics **16**, e1637.
Isserlis, L. (1918), Biometrika **12**, 134.
Jeffries, C. M., J. Ilavsky, A. Martel, S. Hinrichs, A. Meyer, J. S. Pedersen, A. V. Sokolova, and D. I. Svergun (2021), Nature Reviews Methods Primers 2021 1:1 **1**, 1.
de Jeu, W. H. (2016), *Basic X-Ray Scattering for Soft Matter* (Oxford University Press).
Knight, C. J., and J. S. Hub (2015), Nucleic Acids Research **43**, W225.
Kotlarchyk, M., and S.-H. Chen (1983), The Journal of Chemical Physics **79**, 2461.
Krueger, S. (2022), Current opinion in structural biology **74**, 102375.
Köfinger, J., and G. Hummer (2013), Physical Review E - Statistical, Nonlinear, and Soft Matter Physics **87**, 052712.
Larsen, A. H. (2018), "Analytical tools for structure determination of protein complexes with small-angle scattering,".
Larsen, A. H., E. Brookes, M. C. Pedersen, J. J. K. Kirkensgaard, and J. Ilavsky (2023), Journal of Applied Crystallography **56**, 1287.
Larsen, A. H., J. S. Pedersen, and L. Arleth (2020), Journal of Applied Crystallography **53**, 991.
Li, X., C. Do, Y. Liu, L. Sánchez-Diáz, G. Smith, and W. R. Chen (2014), Journal of Applied Crystallography **47**, 1901.
Lindner, P., and J. Oberdisse (2024), *Neutrons, x-rays, and light : scattering methods applied to soft condensed matter* (Elsevier).
Linse, J. B., and J. S. Hub (2023), Communications Chemistry 2023 6:1 **6**, 1.
Liu, H., R. J. Morris, A. Hexemer, S. Grandison, and P. H. Zwart (2012), Acta Crystallographica Section A: Foundations of Crystallography **68**, 278.
Lytje, K., and J. S. Pedersen (2025), Journal of Applied Crystallography **58**, 1332.
Matthews, B. W., and L. Liu (2009), Protein Science **18**, 494.
Mühlbauer, S., D. Honecker, Élio A. Périgo, F. Bergner, S. Disch, A. Heinemann, S. Erokhin, D. Berkov, C. Leighton, M. R. Eskildsen, and A. Michels (2019), Reviews of Modern Physics **91**, 015004.
Narayanan, T., M. Sztucki, P. V. Vaerenbergh, J. Léonardon, J. Gorini, L. Claustre, F. Sever, J. Morse, and P. Boesecke (2018), Journal of Applied Crystallography **51**, 1511.
Park, S., J. P. Bardhan, B. Roux, and L. Makowski (2009), The Journal of Chemical Physics **130**, 10.1063/1.3099611.
Pauw, B. R., A. J. Smith, T. Snow, N. J. Terrill, and A. F. Thünemann (2017), Journal of Applied Crystallography **50**, 1800.
Pedersen, J. S. (1997), Advances in Colloid and Interface Science **70**, 171.
Pedersen, J. S., C. L. Oliveira, H. B. Hübschmann, L. Arleth, S. Manniche, N. Kirkby, and H. M. Nielsen (2012), Biophysical Journal **102**, 2372.
Pedersen, J. S., D. Posselt, and K. Mortensen (1990), Journal of Applied Crystallography **23**, 321.
Pedersen, J. S., and P. Schurtenberger (1996), Macromolecules **29**, 7602.
Poitevin, F., H. Orland, S. Doniach, P. Koehl, and M. Delarue (2011), Nucleic Acids Research **39**, W184.
Porod, G. (1951), Kolloid-Zeitschrift **124**, 83.
Porod, G. (1953), Kolloid-Zeitschrift **133**, 51.
Prince, E. (2004), *International Tables for Crystallography, Volume C: Mathematical, Physical and Chemical Tables* (Springer Netherlands).
Quilez, I. (2014), "Spherical harmonics visualization. this work is licensed under the creative commons attribution 3.0 international license. to view a copy of this license, visit https://creativecommons.org/licenses/by-sa/3.0/.".
Sader, K., D. Studer, B. Zuber, H. Gnaegi, and J. Trinick (2009), Ultramicroscopy **110**, 43.
Sakurai, J. J., and J. Napolitano (2017), *Modern Quantum Mechanics*, 2nd ed. (Cambridge University Press).
Sears, V. F. (1992), Neutron News **3**, 26.
Shinohara, Y., and Y. Amemiya (2015), urn:issn:1600-5767 **48**, 1660.
Spinozzi, F., F. Carsughi, P. Mariani, C. Teixeira, and L. Q. Amaral (2000), Journal of Applied Crystallography **33**, 556.
Stuhrmann, H. B. (1970), Acta Crystallographica Section A **26**, 297.
Svaneborg, C., and J. S. Pedersen (2012), The Journal of Chemical Physics **136**, 10.1063/1.3682778.
Svergun, D., C. Barberato, and M. H. J. Koch (1995), Journal of Applied Crystallography **28**, 768.
Svergun, D. I., M. H. J. Koch, P. A. Timmins, and R. P. May (2013), *Small Angle X-Ray and Neutron Scattering from Solutions of Biological Macromolecules*, 1st ed. (Oxford University Press).
Traube, J. (1895), Ber. Dtsch. Chem. Ges **28**, 2722.
Trewhella, J., P. Vachette, and A. H. Larsen (2024), IUCrJ **11**, 10.1107/S205225252400486X.
Wiedenmann, A. (2001), Physica B: Condensed Matter **297**, 226.
Zernike, F., and J. A. Prins (1927), Zeitschrift für Physik **41**, 184.
Zimm, B. H., and W. H. Stockmayer (1949), The Journal of Chemical Physics **17**, 1301.